PAPER

Check for updates

Biowaste valorization: multifunctional hybrid lignin/TiO$_2$ nanostructures for bacterial-biocide disinfection and dye removal†

Marica Gallo,[a] Virginia Venezia, *[ab] Marica Muscetta, *[a] Rossella Grappa,[a] Mariavittoria Verrillo,[c] Gianluca Landi,[d] Raffaele Marotta[a] and Giuseppina Luciani [a]

An urgent goal is to enhance the economic and environmental value of biowaste *via* recycling and conversion techniques. Lignin, a plentiful plant polymer, holds significant potential for the development of sustainable multifunctional materials. Despite its advantages in terms of red-ox and pollutant adsorption properties, challenges in lignin valorization must address its chemical complexity and tendency to aggregate in water. We demonstrate that lignin and TiO$_2$ can be intimately combined through a versatile *in situ* hydrothermal strategy to obtain hybrid multifunctional nanostructures with tunable functionalities. An in-depth physicochemical analysis elucidates the structure–property–function correlations. The synergistic combination of lignin and TiO$_2$ in hybrid nanoparticles enhances ROS-scavenging/generating properties. Indeed, a lignin content of 20% wt/wt within nanostructures (TiO$_2$_DL200 sample) resulted in nanoparticles with improved antibacterial/antimycotic properties (15 mm increase in the diameter of bacterial growth inhibition (DDK) and 3-fold decrease in the minimum inhibitory concentration (MIC) against fungi compared to neat TiO$_2$ nanoparticles and around 1.3 mm DDK increase and 3-fold MIC decrease against fungi compared to neat lignin) and 90% radical scavenging activity in only 2 minutes. In addition, TiO$_2$_DL200 nanoparticles achieved nearly 80% and 90% removal of methylene blue (MB) and fuchsin (F) dyes, respectively, by adsorption within 5 minutes. Conversely, by tuning the lignin content within the hybrid nanomaterial, a trade-off between the adsorption capacity and the photocatalytic activity is achieved, with MB and F removal efficiencies exceeding 80% in 120 minutes under UV-A conditions for TiO$_2$_DL50. These outcomes prove the potential uses of the obtained hybrid nanoparticles as antioxidant, antibacterial and antifungal additives and for the decontamination of dyes in water remediation.

Environmental significance

Recycling or converting biowaste is advantageous both from environmental and technological perspectives. Biowaste such as lignin may be converted into innovative materials using different methods. Herein, by using a ceramic templating approach, TiO$_2$ and lignin have been intimately combined into hybrid nanostructures, tuning the functionalities by adjusting the lignin amount. Multifunctional nanomaterials with simultaneous antioxidant, antimicrobial and antifungal activities, as well as promising performance for the adsorption and photodegradation of organic pollutants from wastewater have been obtained. At lower lignin content, the nanostructures exhibit pollutant adsorption and photocatalytic degradation, while at higher lignin content antioxidant and UV-blocking properties prevailed. This design underscores the potential applications of such materials and highlights the significant environmental impact of reusing biowaste with tailored functional properties.

[a] DICMaPI, Department of Chemical, Materials and Industrial Production Engineering, University of Naples Federico II, Naples, Italy.
E-mail: virginia.venezia@unina.it, marica.muscetta@unina.it
[b] DiSt, Department of Structures for Engineering and Architecture, University of Naples Federico II, Naples, Italy
[c] Department of Agricultural Science, University of Naples Federico II, Portici, Italy
[d] Institute of Sciences and Technologies for Sustainable Energy and Mobility-CNR, Naples, Italy
† Electronic supplementary information (ESI) available. See DOI: https://doi.org/10.1039/d4en00091a

1. Introduction

The development of novel strategies that enhance the economic and environmental value of biowaste (BW) through recycling or conversion methods is beneficial from both an environmental and technological point of view.[1] Indeed, BW can be transformed into a wide range of end-use products and novel functional materials through various chemical, physical, and biological approaches.[2–4] In biowaste, lignin, is one of the most abundant components available for possible

This journal is © The Royal Society of Chemistry 2024

Environ. Sci.: Nano, 2024, **11**, 2127–2144 | **2127**

valorization, being the second most common plant polymer after cellulose.[5] Lignin is an amorphous, highly branched polymer characterized by high aromaticity:[6,7] it contains numerous hydrophilic and active functional groups (such as hydroxyl, carbonyl and methoxyl groups), which confer this polymer several interesting properties, including antibacterial, antioxidant, and UV-blocking properties, or metal ion chelation capability.[8,9] These intriguing features, coupled with lignin's renewability, broad availability and biodegradable nature, make this biopolymer a highly appealing option for the design of multifunctional materials for potential bio-sustainable advanced applications,[7] including catalysis, production of smart composites, carbon fiber adsorbents, drug nanocarriers or a precursor for the synthesis of metal oxide nanomaterials.[10]

Despite its high potential, the extraction processes, as well as the starting biomass material, strongly influence the properties of the biopolymer. These drawbacks, along with the bulk lignin's tendency to form aggregates in an aqueous environment, have so far greatly limited the valorization processes of this intriguing material, relegating this biopolymer to the role of waste.[11,12] Indeed, only 2% of the world annual production of lignin is converted into high-value chemical compounds, while the majority is used for low-tech applications such as fuel.[13]

With the aim to overcome some of these issues, several authors have recently proposed the design of lignin-based nanostructured materials, including nanoparticles, nanofibers, nanofilms, and nanotubes, also combining them with inorganic oxides.[14–16] The obtained materials are non-toxic and appear more stable in aqueous solution in comparison to the bulk lignin.[17]

The combination of bioderived organic moieties with either an inorganic or an organic component can improve the intrinsic features of the inorganic phase. Specifically, in view of their marked biocompatibility, tunable size, shape, and porosity as well as functional versatility, several inorganic nanoparticles represent valid candidates for the development of multifunctional nanomaterials with modulable properties.[18,19] Among them, titanium dioxide (TiO_2) is one of the most interesting, due to its availability and low toxicity; specifically, TiO_2 could interact with lignin through the formation of metal–ligand complexes, hydrogen bonding, electrostatic interactions, and van der Waals force, thus impacting the overall morphology and the activity of the final material.[20,21]

For instance, TiO_2–lignin hybrid nanomaterials have been previously developed as additives to enhance the mechanical and the functional properties of polymeric materials,[22,23] as metal ion adsorbers,[24] as antimicrobial or antioxidant agents,[25–27] as (photo)catalysts,[28–30] and as UV-protecting agents for cosmetic applications.[25,31,32]

However, to our knowledge, most of the scientific literature on this subject has concentrated on the *extra situ* modification of prepared TiO_2 nanoparticles and often includes calcination steps, leading to a partial degradation of lignin.[33–35] These aspects have been overcome in this work. Indeed, the molecular conjugation of biomacromolecules and inorganic components into hybrid nanostructures has been carried out.

In this context, the ceramic templated approach has proven to be an extremely effective strategy to produce hybrid organo–inorganic nanostructures, even enhancing the intrinsic properties of bioderived organic moieties, selectively driving its function.[19]

Indeed, TiO_2 can be proposed as a biomimetic templating agent for controlling and modulating the stability and the reactivity of bulk lignin.

In the present work, hybrid multifunctional lignin/TiO_2 nanomaterials added with different amounts of dealkaline lignin (DL) during the synthesis, were designed, and prepared through an *in situ* method based on the hydrothermal wet chemistry approach.

In this study, the ceramic templated approach was applied with the lignin biopolymer, demonstrating its effectiveness in developing reproducible hybrid systems with remarkable multifunctional capabilities across several applications. Significantly, this method allows the modulation of the optical, physico-chemical, and structural properties of the nanoparticles, allowing the final application of the nanoparticles to be tailored to the amount of lignin used during the synthesis. A deep physico-chemical investigation of the nanohybrids was thoroughly carried out using FTIR, TGA, TEM, DLS, zeta potential, BET, XRD and UV-vis DRS analyses, while their functional properties, in terms of antioxidant, antimicrobial and antifungal activities, were evaluated using different assays and antimicrobial/antimycotic tests and compared with those of neat TiO_2 and lignin.

Finally, the adsorption capacity and the photocatalytic activity of the nanoparticles were evaluated, to verify their potential as active agents for the decontamination of common organic dyes in wastewater (*i.e.*, methylene blue and fuchsin). Fuchsin and methylene blue, chosen as probe pollutants being largely reported in the literature, have indeed wide industrial application, as dyes in the textile field. The interest in the removal of these compounds from water derives from the serious environmental issues due to high toxicity and accumulation in the environment.[36,37]

The durability of the tested nanomaterials in dye removal was evaluated both for adsorption and photocatalytic purposes through different reusability tests. The proposed approach offers a promising solution to turn biowaste into valuable multifunctional materials with improved redox behaviour and managing water quality. The dual focus on evaluating antibacterial/antifungal efficacy and dye removal capability is in line with our aim to develop a material with multiple applications starting from a biowaste. The choice to integrate these functionalities demonstrates the versatility and potential applications of such hybrid nanomaterials in addressing both environmental and health concerns.

2. Experimental section

2.1 Materials

Titanium isopropoxide (TTiP) (CAS Number 546-68-9), isopropanol (CAS Number 67-63-0), acetic acid (CAS Number 64-19-7), triethylamine (TEA) (CAS Number 121-44-8), Folin–

2128 | *Environ. Sci.: Nano*, 2024, **11**, 2127–2144

This journal is © The Royal Society of Chemistry 2024

Ciocâlteu reagent (CAS Number F9252), 2,2′-azino-bis(3-ethylbenzthiazoline-6-sulfonic acid) diammonium salt (ABTS) (CAS Number 30931-67-0), potassium persulfate (CAS Number 7727-21-1), 2,2-diphenyl-1-picrylhydrazyl (DPPH) (CAS Number 1898-66-4), methylene blue (CAS Number 61-73-4) and sodium carbonate (CAS Number 497-19-8) were purchased from Sigma Aldrich (Milan, Italy). Dealkaline lignin (CAS Number 8061-51-6) was purchased from Tokyo Chemical Industry Co, Ltd (Zwijndrecht, Belgium) and basic fuchsin (70% pure) (CAS Number 632-99-5) was purchased from ThermoFisher Scientific (Rome, Italy). All chemicals were used as received without further purification treatment.

2.2 Synthesis of hybrid TiO₂_DL nanoparticles

Bare TiO_2 and hybrid TiO_2_DL nanoparticles (TiO_2_DL NPs) were prepared in the absence and in the presence of dealkaline lignin (DL), respectively. Specifically, neat TiO_2 nanoparticles have been prepared under the same synthesis conditions as those employed for hybrid nanoparticles, but without DL in the reaction batch.

The synthesis was conducted *via* a hydrothermal process based on an experimental procedure previously developed by our group.[38] Briefly, a solution of the TiO_2 precursor was prepared *via* dropwise addition of 6 mL of 1.69 M titanium(IV) isopropoxide (TTiP) in 2-propanol to 31.3 mL of an aqueous solution of acetic acid at pH = 1.5. This mixture was stirred at room temperature and at 400 rpm for one day, until a TiO_2 colloidal suspension was obtained. Then, 25, 50, 100 or 200 mg of DL was added to the TiO_2-sol suspension, to obtain TiO_2_DL25, TiO_2_DL50, TiO_2_DL100 and TiO_2_DL200, respectively. Subsequently, triethylamine (TEA) was added dropwise to the mixtures until pH = 7.0. The obtained suspensions were sealed within Teflon recipients, in which the liquid volume corresponded to 75% of the total volume, and they were placed into a circulating oven (MEMMERT 30-1060) and maintained at 120 °C for 18 h. The final sample was recovered by centrifugation, by means of an SL 16 Thermo Fisher Scientific centrifuge, at 11 500 rpm (14 000 × *g*) for 10 min and then washed 3 times with distilled water after each centrifugation step. The obtained nanoparticles were dried at 80 °C overnight to carry out some of the following experiments.

2.3 Preparation of DL solutions

Solutions containing only DL were prepared and subjected to the same solvothermal treatment used for the nanoparticle synthesis to evaluate any changes in composition, structure and functionality undergone by neat lignin during the thermal process (DL T). Briefly, a specific amount of lignin was added with respect to the same nominal percentage of organic material used for the preparation of hybrid nanoparticles (TiO₂_NPs). Indeed, the volume of distilled water was equal to the total volume of reagents used (water, titanium isopropoxide, acetic acid, isopropyl alcohol, and triethylamine) in the nanoparticle synthesis.

The prepared solutions were characterized by DL/water ratios of 0.33, 0.66, 1.33 and 2.66 (wt/vol).

Then, they were stirred for 1 hour and underwent hydrothermal treatment for 24 hours at 120 °C.

The recovered samples are indicated below with the following labels: DL T25, DL T50, DL T100 and DL T200. The obtained DL solutions were dried at 80 °C overnight to carry out some of the following experiments.

2.4 Physicochemical characterization of TiO₂_DL hybrid nanoparticles

Fourier transform infrared spectroscopy (FTIR) analysis was carried out to unveil the presence of DL within the hybrid nanomaterial. A Nexus FTIR spectrometer equipped with a DTGS KBr (deuterated triglycine sulfate with potassium bromide windows) detector was employed. FT-IR absorption spectra were obtained in the 4000–400 cm⁻¹ interval, by using 2 cm⁻¹ as the spectral resolution. All the samples were prepared by mixing 200 mg of KBr and 1 mg of dried sample powders and pressing them into pellets 13 mm in diameter. In addition, KBr was used as a reference for each sample.

Thermogravimetric (TGA/DSC) analyses were conducted to investigate the thermal behavior of samples by using a TA instrument simultaneous thermo-analyser SDT Q600 (TA Instrument, New Castle, DE, USA). To evaluate the weight loss of each sample and, therefore, the DL content in hybrid nanoparticles, TGA analysis was carried out according to the Standard Test Methods for Proximate Analysis. Briefly, 10 mg of each sample were placed in a platinum pan and tested in inert atmosphere. To eliminate the contribution of moisture, each sample was heated to 110 °C at a rate of 20 °C min⁻¹. The test was conducted in the temperature range of 110 °C to 970 °C at a heating rate of 50 °C min⁻¹, and the samples were then kept at 970 °C for 7 minutes. Therefore, the samples were cooled again from 970 °C to 600 °C with a heating rate of 20 °C min⁻¹.

The percentage of organic content in bare TiO_2 and TiO_2_DL materials was evaluated as follows:

$$\text{Organic content (\%)} = \frac{W(110\ °C) - W(970\ °C)}{W(110\ °C)} \times 100 \quad (1)$$

where $W(110\ °C)$ and $W(970\ °C)$ are the weight at 110 °C and 970 °C of the same sample, respectively. Besides, the percentage of dealkaline lignin (DL) content in the hybrid sample was calculated as follows:

$$\text{DL (\%)} = \frac{W_{TiO_2}(970\ °C) - W_{TiO_2\_DL}(970\ °C)}{W_{TiO_2}(970\ °C) - W_{DL}(970\ °C)} \times 100 \quad (2)$$

where $W_{TiO_2}(970\ °C)$, $W_{TiO_2\_DL}(970\ °C)$ and $W_{DL}(970\ °C)$ are the weight at 970 °C of the bare TiO_2, hybrid TiO_2_DL (25, 50, 100, or 200) and dealkaline lignin (DL), respectively, each calculated from eqn (2).

The morphological properties of the obtained nanoparticles were evaluated using transmission electron microscopy (TEM). The samples were prepared by putting a drop of the nanohybrid suspension on one side of a 200-mesh carbon-coated copper

This journal is © The Royal Society of Chemistry 2024

Environ. Sci.: Nano, 2024, **11**, 2127–2144 | **2129**

grid. Bright-field TEM images were obtained on the dried sample by using an FEI TECNAI G2 200 kV S-Twin microscope (Thermo Fisher Scientific, Waltham, USA) equipped with lenses for high-resolution imaging. The size distribution of the nanoparticles was evaluated by using ImageJ software and measuring at least 100 microscopy images.

Dynamic light scattering (DLS) and zeta potential measurements were conducted by using a Zetasizer Lab (Malvern, Panalytical) to investigate the size distribution and the surface charge of nanoparticles, respectively. All the samples were diluted up to a concentration of approximately 0.025% w/v by using distilled water, which corresponded to a final nanoparticle concentration of 0.25 mg ml^{-1}. In addition, the pH value is around 5.5 in all cases. A detecting angle of 90, a default refractive index ratio of 1.33 and 5 runs for each measurement (1 run lasting 100 s) were used in the calculations of the particle size distribution. The zeta potential was calculated by the Smoluchowski model. Each investigation was carried out three times to assess sample reproducibility.

The surface properties were determined *via* N$_2$ adsorption at −196 °C starting from $P/P_0 = 5 \times 10^{-6}$ using a Quantachrome Autosorb 1-C instrument (Quantachrome, Anton Paar Italia, Rivoli, Italy). Before the analysis, the samples were degassed under high vacuum at 120 °C for 4 h. The BET method (P/P_0 range from 0.05 to 0.3) was adopted for the calculation of the specific surface area (S_{BET}), while the total pore volume (V_{TOT}) was computed using Gurvitch's rule (at $P/P_0 = 0.995$). Finally, the pore size distribution was evaluated *via* the application of the BJH model to the desorption branch of the isotherm.

X-ray diffraction (XRD) experiments were carried out with a Malvern PANalytical diffractometer (Malvern, UK) with a nickel filter and Cu Kα radiation, to define the crystalline phases of the TiO$_2$ component in the hybrid nanomaterial. The average crystal size (τ) was evaluated through the Scherrer formula:

$$\tau = \frac{K\lambda}{\beta \cos\theta} \tag{3}$$

where τ is the mean size of the crystallite domains, K is a dimensionless shape factor, λ is the X-ray wavelength, β is the broadening at half the maximum intensity (FWHM), and θ is the Bragg angle.

UV-vis diffuse reflectance spectroscopy (DRS) measurements were carried out using a UV-2600i UV-vis spectrophotometer, 230 V (Shimadzu, Milan, Italy), equipped with an integrating sphere ISR-2600Plus operating in a wavelength range of 220–1400 nm. Barium sulfate was used as a reflectance standard. The measured intensity was expressed as the value of the Kubelka–Munk function, $F(R)$, while the direct band-gap energy value was evaluated according to the Tauc-plot linearization of $(F(R)h\nu)^2$ against $h\nu$.

The determination of the zero points of charge (pH$_{zpc}$) of the materials involved the examination of the fluctuations in zeta potential values at various pH levels, by following a procedure reported in the literature.[39] The measurements were conducted on solutions with a 1 mg mL^{-1} solid concentration. The pH of the solutions was modified by employing 0.1 M HNO$_3$ and 0.1 M NaOH (ranging from pH = 2 to pH = 11). The samples were subjected to stirring for 1 hour, followed by an overnight settling period. Then, the zeta potential values were determined at T = 25 °C using a Zetasizer Lab instrument (Malvern, Panalytical).

2.5 Functional characterization of TiO$_2$_DL hybrid nanoparticles and DL solutions

The quantitative determination of phenols and polyphenols was performed through colorimetric determination using the Folin–Ciocâlteu reagent (FCR). The test involves the detection of a blue chromophore that is formed when FCR reacts with a substance that contains phenolic groups; the maximal absorbance is dependent on the quantity of phenolic compounds. Specifically, at pH 10 (achieved by adding a solution of Na$_2$CO$_3$), the interaction between FCR and phenols takes place under a basic environment. Phenols are dissociated (phenolate anion) and able to decrease FCR under these conditions.

Each nanoparticle aqueous solution is added at a final concentration of 0.075 mg ml^{-1} to a solution containing FCR reagent, 75 g L^{-1} of Na$_2$CO$_3$, and water in a volumetric ratio of 1 : 3 : 14.

After the combination has been held at 40 °C for 30 minutes, the absorbance at 765 nm is measured.[40] The results are expressed as mg of gallic acid equivalent per gram of the sample, with gallic acid serving as the reference standard. The tests were carried out in triplicate.

The antioxidant activity of TiO$_2$_DL hybrid nanoparticles and DL solutions was evaluated using ABTS analysis. This method is based on the oxidation of 2,2′-azino-bis(3-ethylbenzthiazoline-6-sulfonic acid) (ABTS) diammonium salt by potassium persulfate to form a radical cation (ABTS$^{·+}$). In detail, a concentration of ABTS aqueous solution at 7 mM was prepared, and the ABTS radical cation (ABTS$^{·+}$) was generated by adding 2.45 mmol L^{-1} of potassium persulfate and allowing the reaction solution to rest in the dark at room temperature for 12–16 hours before use. Subsequently, a working solution of ABTS$^{·+}$ was prepared by diluting 10 mL of the stock solution in 800 mL of a water/ethanol solution (50 : 50, v/v), with absorbance at 734 nm on the UV-vis spectrophotometer ranging between 0.75 and 0.80.

For the sample preparation, 2 mg of each sample were dissolved in 2 mL of water, and 100 μL of this solution were added to 1.9 mL of the ABTS$^{·+}$ working solution. The mixture was stirred in the dark for 2 minutes to promote the reaction between the polyphenols and the ABTS$^{·+}$ free radicals. The reaction was carried out in the dark to avoid interference from light-induced reactions. Absorbance readings were taken at 734 nm using a Perkin Elmer Lambda 25 UV/vis spectrometer. The results were expressed as Trolox equivalent antioxidant capacity (TEAC) based on a linear calibration curve of Trolox in the range of 0.1 to 80 mg L^{-1} (R^2 = 0.996). The measurements were performed in triplicate.

2130 | *Environ. Sci.: Nano*, 2024, **11**, 2127–2144

This journal is © The Royal Society of Chemistry 2024

The antioxidant activity of the obtained nanostructures has been evaluated also by means of the DPPH (2,2-diphenyl-1-picrylhydrazyl) free radical scavenging method, as described elsewhere.[41] Briefly, 1 mL of each nanoparticle aqueous solution at 1 mg mL^{-1} is mixed with 2 mL of 100 μM DPPH methanol solution. The mixture is kept in the dark for 30 min and the absorbance at 517 nm is measured using a UV-vis spectrophotometer, 230 V (Shimadzu, Milan, Italy), equipped with an integrating sphere ISR-2600Plus operating in a wavelength range of 220–1400 nm.

The percentage of DPPH free radical scavenging activity is calculated following eqn (4):

$$\text{DPPH scavenging effect (\%)} = \frac{A_{\text{DPPH}} - A_{\text{Sample}}}{A_{\text{DPPH}}} \times 100 \quad (4)$$

where A_{DPPH} and A_{Sample} are the absorbance of the methanolic solution of DPPH and the absorbance of the sample, respectively. All the measurements were performed in triplicate.

The antimicrobial activity was performed using the disk diffusion test (DDK) and the broth microdilution method (MIC).[42] The microbial strains used were *Staphylococcus aureus ATCC 6538P*, *Enterococcus faecalis ATCC 29212*, *Bacillus cereus ICE170*, and *Listeria monocytogenes ATCC19115* as Gram (+) bacterial strains and *Salmonella typhi ATCC14028* and *Escherichia coli ATCC 33780* as Gram (−) ones. Briefly, the MIC test was performed using Mueller–Hinton broth medium with sterile polypropylene 96-well microtiter plates. The microbial inoculum size used was 1×10^6 cells per mL (NCCLS, 1993). Serial double dilutions of various samples were made to obtain concentrations ranging from 10 to 1000 μg mL^{-1}. Then, bacterial cells were inoculated from an overnight culture at a final concentration of approximately 5×10^5 CFU mL^{-1} per well and incubated with different samples overnight at 37 °C. The MIC values were defined as the lowest tested nanoparticle concentration that inhibited the growth of bacterial cells after 24 hours of incubation at 37 °C. On the other hand, the disk diffusion method (DDK) was performed according to the standard method of the National Committee for Clinical Laboratory Standards (NCCLS). Briefly, the suspension of each microbial strain was transferred onto nutrient agar and incubated at 37 °C for 24 hours. The inoculum was standardized by transferring colonies from the nutrient agar to sterile saline solution to achieve a concentration of 10^8 CFU mL^{-1} (0.5 McFarland). Then, 200 μL of cells were placed on Mueller–Hinton agar, and different disks (6.0 mm diameter) were incubated with 20 μL of each NP at 37 °C for 24 hours. Ampicillin (30 μg) and clavulanic acid (AMP–CA) were used as positive controls, while bovine serum albumin (BSA) was used as a negative control. Finally, the inhibition diameters were calculated by measuring the size of the inhibition zones (mm).

The antifungal activity of the nanoparticles was measured using a modified microdilution method that allowed determining the MIC value of the samples that inhibit the growth of *Candida albicans* and *Aspergillus flavus*

microorganisms.[43] Amphotericin B, an antifungal medication used for serious fungal infections, has been used as a positive control. The nanoparticle dispersion was diluted in microtiter plates containing culture medium[44] at different concentrations, ranging from 2 mg L^{-1} to 0.05 mg L^{-1}. After sample dilution, a standard amount of the tested yeast was inoculated onto the microtiter plates, so that the inoculum density in the wells was 10^6 CFU mL^{-1}. After 36 hours of incubation at 37 °C, the MIC was recorded as the lowest concentration of the agent that inhibited the visible growth of the microorganisms.

2.6 Evaluation of adsorption + photocatalytic degradation of dyes

As probe pollutants, methylene blue (MB) and fuchsin (F) dyes were used to evaluate the photocatalytic efficacy of the samples. Photocatalytic experiments were performed in 50 mL glass beakers illuminated by a high-pressure mercury lamp (Helios Italquartz, 125 W). The lamp was positioned at 10 cm distance from the beakers (see Fig. S1† for the schematic representation of the experimental set-up), in which a suitable amount of TiO$_2$ or TiO$_2$_DL nanoparticles (1 g L^{-1}) was added to a 0.02 mM solution of dyes (*i.e.*, MB or F) at pH = 5.0 and T = 25 °C. To obtain the adsorption–desorption equilibrium, the aqueous suspension was stirred continuously at 500 rpm for 60 minutes under dark conditions. During the experiment, a suitable volume (3 mL) of liquid samples was taken at predetermined intervals and then centrifuged at 5000 rpm for 5 minutes to remove the solid. As previously reported,[45,46] a spectrophotometer Cary UV-vis (Agilent Technologies) was used to measure the absorbance of MB (λ = 660 nm) and F (λ = 540 nm) for estimating the dye removal degree. The adsorption percentage was estimated through eqn (5):

$$\% \text{ dye adsorption} = \frac{C_0 - C}{C_0} \cdot 100 \quad (5)$$

Furthermore, the adsorption capacity was determined through the following formula (6):

$$q_e = \frac{C_0 - C_e}{\frac{m_{\text{hybrid nanomaterial}}}{V_{\text{sol}}}} \quad (6)$$

where: C_0, C and C_e (mg L^{-1}) are the initial concentration of dye, the concentration of dye at a certain time t (min) and the equilibrium concentration after adsorption, respectively; moreover, $m_{\text{hybrid nanomaterial}}$ (g) is the amount of the hybrid nanomaterial used and V_{sol} (L) is the solution volume. Some experiments were performed at different amounts of the nanomaterials, and the obtained data were analysed to determine the adsorption kinetics by fitting them using the linearized form of the Langmuir adsorption isotherm (7):

$$\frac{C_e}{q_e} = \frac{1}{K_L \cdot q_m} + \frac{C_e}{q_m} \quad (7)$$

where K_L is the bonding energy adsorption (L/mg) and q_m is the maximum adsorbed dye amount (mg g^{-1}).

This journal is © The Royal Society of Chemistry 2024

Environ. Sci.: Nano, 2024, **11**, 2127–2144 | **2131**

Likewise, the pseudo-first-order kinetics was used to study the photocatalytic degradation phenomenon (8):

$$\mathrm{Ln}\left(\frac{C}{C_0}\right) = -k \cdot t \qquad (8)$$

where k is the pseudo-first-order kinetic constant (1/min) and t is the irradiation time (min).

To evaluate the reusability of some of the nanomaterials as adsorbents, the nanoparticle suspension was left to settle after each test until there was a full separation of the solid and liquid phases. Subsequently, the supernatant was removed, and the following washing procedure was carried out: (1) washing three times with distilled water, (2) three times with methanol, (3) three times with distilled water. Then, the solid material was dried overnight at 80 °C and tested for another adsorption experiment. Finally, to assess the reusability of the hybrid nanomaterials in the dye adsorption + photocatalytic removal process, at the end of some experimental runs, the suspension was allowed to settle until a complete separation between the solid and liquid phases occurred. Subsequently, the supernatant was removed, while a fresh solution, with an equivalent dye concentration, was added. The procedure was replicated three times.

3. Results and discussion

3.1 Physico-chemical characterization of hybrid TiO₂_DL nanoparticles

FT-IR analysis was performed on all the samples to assess the lignin presence within the hybrid nanomaterials and to investigate the nature of the interaction with the inorganic skeleton as well.[25,34,47,48] Fig. 1 shows the comparison among FT-IR spectra of DL after hydrothermal treatment (DL T), bare TiO₂ and the hybrid nanomaterials. The infrared spectrum of

Fig. 1 FTIR spectra of: A) TiO₂, B) TiO₂_DL25, C) TiO₂_DL50, D) TiO₂_DL100, E) TiO₂_DL200, and F) DL T.

neat TiO₂ nanoparticles (Fig. 1A) exhibits the peculiar attributes of TiO₂. Indeed, the wide band within the 500–850 cm⁻¹ range is a result of the stretching vibrations of Ti–O and Ti–O–Ti bonds.[34] Furthermore, the stretching band observed in the 3100–3600 cm⁻¹ range can be ascribable to hydroxyl groups from residual bound TEA, absorbed water, and surface-bound Ti–OH bonds.[47] The lignin biopolymer is primarily composed of three phenylpropanoic alcohol units known as monolignols: synapyl alcohol (3-methoxy-4-hydroxymethyl alcohol), coniferous alcohol (3-methoxy-4-hydroxymethyl alcohol), and *p*-coumarin alcohol (4-hydroxymethyl alcohol).

Table S1† shows FTIR assignments related to lignin chemical structure.[25,34,48] After the hydrothermal treatment, the main structure of the original lignin was retained well, with only slight changes (Fig. S2†), as previously reported.[49,50]

Specifically, the DL T spectrum (Fig. 1F) exhibits a much stronger –OH stretching band at 3420 cm⁻¹ with respect to that of the DL spectrum, suggesting the considerable presence of phenols in the lignin structure after the hydrothermal treatment. The C–H stretching in the –CH₃ and –CH₂ groups can be detected at around 2940 and 2840 cm⁻¹, respectively (Fig. 1F).[48] On the other hand, aromatic skeletal vibrations have been recorded in the 1600–1000 cm⁻¹ range, specifically at around 1600, 1520, 1460, 1420, and 1120 cm⁻¹.[34] In addition, the band at around 1710 cm⁻¹ is commonly attributed to C=O stretching, while the region between 700 and 900 cm⁻¹ is associated with benzene ring C–H stretching.[25] In addition, it is possible to appreciate other some slight differences with respect to the FTIR spectrum of bare DL (Fig. S2†), including a slight increase of vibration of aromatic rings (1590, 1510 cm⁻¹), the disappearance of aromatic C–O stretching of syringyl units (1350 cm⁻¹), a slight decrease of aromatic C–O stretching of guaiacyl units (1265 cm⁻¹) and a slight increase of phenolic –OH units (1210 cm⁻¹).

On the other hand, FTIR spectra of hybrid TiO₂_DL samples share with DL several bands in the 1600–1000 cm⁻¹ range, and at around 3420 cm⁻¹, especially in the case of TiO₂_DL200 (Fig. 1E), thus proving the presence of DL in the hybrid nanostructures.

The amount of DL effectively incorporated onto/into the hybrid nanomaterial during the synthesis phase was evaluated through TGA analysis, as described in the Experimental section.

TGA curves of DL and DL T samples are shown in Fig. S2, B.† Thermal degradation occurred primarily between 200 and 750 °C in both cases.[50] Even though no macroscopic changes can be appreciated, at a closer look, TGA analysis suggests a slightly higher thermal stability in DL T sample, which can be attributed to the formation of more stable lignin structures. To this regard, DTG curves for the DL samples showed two main degradation peaks (Fig. S2, C†): the first, at approximately 340 °C, is related to aliphatic and oxygen-bonded carbons, and the second at around 740 °C is indicative of stable lignin components. Conversely, DL T samples exhibited three peaks at approximately 220, 380, and
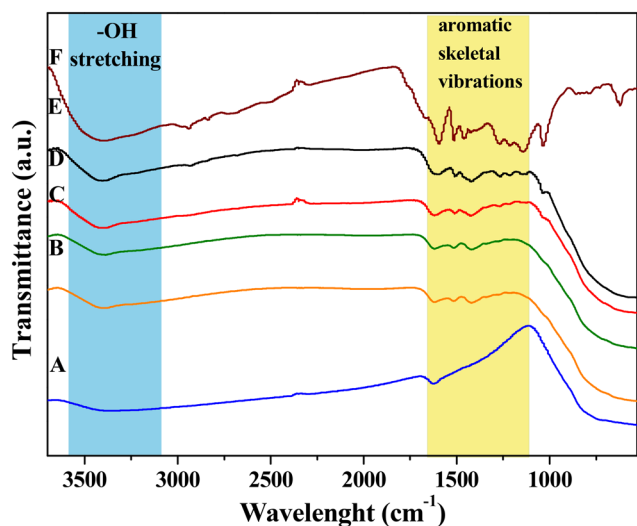
Table 1 % wt DL of hybrid nanoparticles estimated by means of TGA

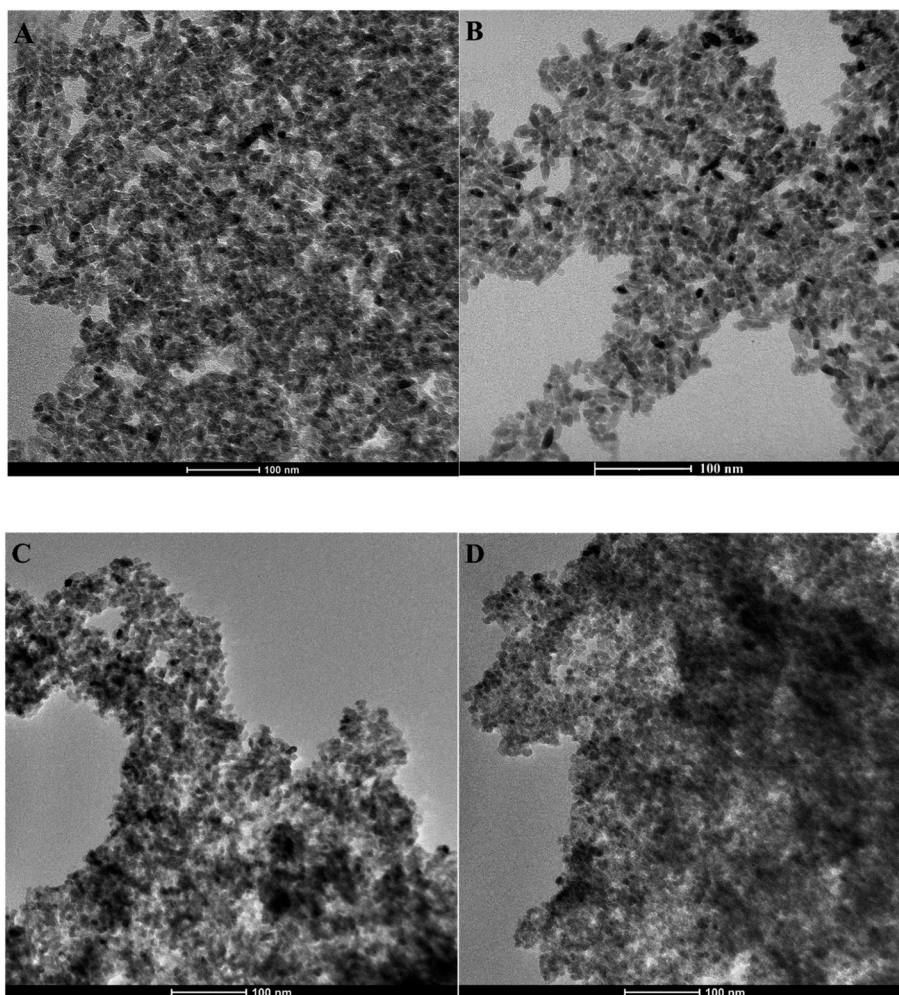| Sample	% wt DL (±0.5%)
TiO$_2$_DL25	1
TiO$_2$_DL50	2
TiO$_2$_DL100	8
TiO$_2$_DL200	19

790 °C. The first peak suggested slight depolymerization of lignin due to the hydrothermal treatment, which generated more reactive intermediates. The second peak at around 380 °C involved the decomposition of aliphatic groups and carbohydrates and was larger than that revealed in the DTG curve of the DL sample due to higher aromatic/polyphenolic content. The third peak at around 790 °C was attributed to the decomposition of polycondensed aromatic moieties. Overall, the hydrothermal treatment had the potential to form new linkages, as indicated by FTIR spectra.

TGA curves of hybrid TiO$_2$_DL samples are shown in Fig. S3† and the amount of DL present in the hybrid nanomaterials was evaluated using eqn (2) provided in the Experimental section.

The calculated values are reported in Table 1 and suggest that the weight percentage of DL contained in the hybrid nanoparticles increases as the amount of lignin used in the synthesis phase increases. In addition, the TGA curves of the nanohybrids showed the largest weight loss in the range of 200–800 °C (Fig. S3†), which corresponded to the main decomposition of DL according to the TGA curve of DL T (Fig. S2, B†).

The TEM micrograph of the bare TiO$_2$ sample (Fig. S4†) reveals rod-like TiO$_2$ nanoparticles with an average size of approximately 30–35 nm, in accordance with our previous studies.[51] On the other hand, TEM pictures of TiO$_2$_DL nanohybrids (Fig. 2) show that hybrid nanoparticles tend to have a spherical shape with an average size of 10 nm, which does not seem to be influenced by the nominal lignin content used in the synthesis. Moreover, no evident phase separation can be appreciated in TEM pictures, suggesting the intimate mixing of organic and inorganic components.

Similar morphological features have been outlined for hybrid nanomaterials obtained through the solvothermal synthesis of TiO$_2$ in the presence of polyphenol-like[38] or poly-hydroxyindole organic components. Indeed, the catechol

Fig. 2 TEM micrographs of A) TiO$_2$_DL25, B) TiO$_2$_DL50, C) TiO$_2$_DL100, and D) TiO$_2$_DL200.

This journal is © The Royal Society of Chemistry 2024

Environ. Sci.: Nano, 2024, **11**, 2127–2144 | **2133**

moieties in these structures can bind Ti^{4+} cations in both monodentate and bidentate conformations,[52] directing crystal growth during the hydrothermal step, thus producing a morphological change with respect to the neat sample. TiO_2_DL nanoparticles look much smaller than bare TiO_2 ones, and the outer surface of a single particle is barely discernible. Neat TiO_2 nanoparticles undergo clustering phenomena (as illustrated in Fig. S4†), potentially induced by van der Waals interparticle aggregation.[53] Extensive aggregation also impacts hybrid systems, as evident in Fig. 2, resulting in the formation of micrometric aggregates due to the unique amphiphilic properties of lignin. Indeed, lignin is a biopolymer with a high molecular weight, marked by the simultaneous presence of polar components such as phenols and carboxyl groups alongside aromatic rings. This chemical structure is responsible for the self-assembly behavior of such supramolecular structures in aqueous solutions, thus leading to the formation of three-dimensional nanostructures.[54,55] In the context of the hybrid synthesis approach, when lignin is adsorbed onto/into the crystalline structure, the supramolecular aggregation of lignin results in the formation of clusters made of hybrid nanoparticles.

DLS experiments were conducted to evaluate the colloidal stability, as well as the self-assembly behavior of neat TiO_2 and TiO_2_DL nanohybrids in aqueous environments. Specifically, TEM analysis suggested that the nanoparticles organize themselves into submicrometric aggregates (Fig. 2), whose mean size, in terms of hydrodynamic diameter (D_h), can be appreciated by means of DLS measurements. The addition of lignin leads to an improvement of D_h, compared to that of neat TiO_2 nanoparticles (Table S2 and in Fig. S5†). Indeed, higher quantities of lignin in TiO_2_Dl00 and TiO_2_DL 200 samples result in the formation of micrometer-sized aggregates, as shown in (Table S2†). These features further suggest the key role of DL in tuning the aggregation phenomena of TiO_2 nanoparticles, which is bound to be strictly related to the presence of the aromatic moieties within the DL chemical structure. Indeed, as the DL content increases, the organic phase may better act as a "binder" for different nanoparticle aggregates through hydrophobic interactions, thus leading to the formation of larger clusters, up to the micron scale (Table S2†).

Zeta potential results provided information about the surface charge of the obtained nanostructures (Table S2†). Overall, the presence of lignin in the nanostructures influences their surface charge, which becomes increasingly negative by increasing the organic phase content during the synthesis phase. When DL gets adsorbed onto/into the TiO_2 crystalline structure, the ionization of acidic functional groups in an aqueous environment (–COOH, –OH linked to aromatic rings) occurs, thus leading to more negative surface charge when a higher DL content is added during the synthesis route.[33,41]

The specific surface area (SSA) of the investigated samples was determined using N_2 physisorption. All the nanoparticles exhibited a type IVb isotherm (Fig. S6†), which is typical of mesoporous materials derived from primary nanoparticle aggregation, and displayed capillary condensation accompanied by hysteresis during desorption, as previously noted in other studies.[56] Table 2 shows the SSA values, the pore volume, and the average pore diameter for neat TiO_2 and hybrid TiO_2_DL nanoparticles. The SSA value of neat TiO_2 nanoparticles is 169 m^2 g^{-1}, in accordance with previous studies,[38] whereas the DL T organic component has a SSA value of about 2 m^2 g^{-1}. All hybrid nanostructures showed lower SSA values with respect to bare TiO_2 ones, except for the TiO_2_DL25 sample. Higher DL content in the reaction solution could result in a greater amount of DL biomolecules on the surface of primary colloidal TiO_2 nanoparticles. This feature also leads to an increase in the number of negative surface charges, as also suggested by zeta-potential values, thus affecting the growth of hybrid materials which are characterized by marked aggregation phenomena and, therefore, by an overall smaller surface. Consequently, as shown in Table 2, the changes in the surface areas of the hybrid nanomaterials compared to bare TiO_2 nanoparticles are accompanied by a slight decrease in the pore diameter and in the total pore volume of the samples. This finding further suggests the pivotal role of DL in influencing the growth and structural organization of TiO_2_DL nanohybrids, ultimately modifying their surface area and porosity.

XRD analysis was conducted to determine the crystalline structure of the inorganic component TiO_2 in the hybrid nanomaterials. The DL T pattern exhibits an amorphous structure, characteristic of the organic components extracted from biomass (Fig. S7†). On the other hand, the diffraction patterns of neat TiO_2 and all TiO_2_DL nanohybrids show a typical profile of anatase, one of the typical crystalline forms of TiO_2, both in terms of peak positions and relative intensities (Fig. S7†), demonstrating that the growth of the

Table 2 Specific surface area (SSA), pore volume and mean pore diameter of DL T, TiO_2 and TiO_2_DL nanoparticles

Sample	Specific surface area (SSA) (m^2 g^{-1}) (±7%)	Pore volume (cm^3 g^{-1}) (±0.02)	Mean pore diameter (Å) (±10%)
DL T	2	Negligible	Negligible
TiO_2	169	0.30	66
TiO_2_DL25	185	0.21	63
TiO_2_DL50	158	0.19	63
TiO_2_DL100	149	0.16	51
TiO_2_DL200	112	0.13	42

2134 | Environ. Sci.: Nano, 2024, **11**, 2127–2144
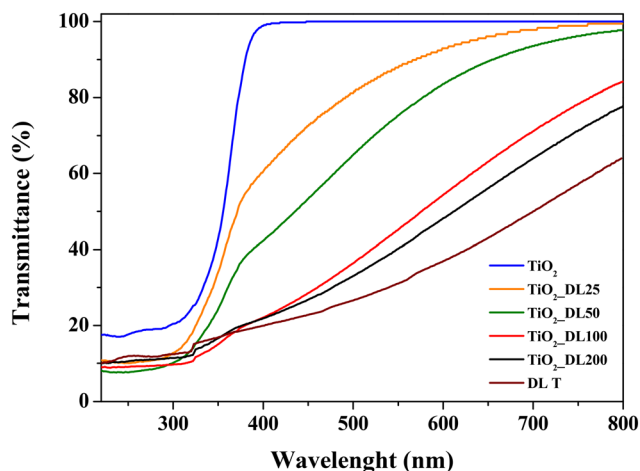
This journal is © The Royal Society of Chemistry 2024

Fig. 3 Transmittance spectra of bare TiO_2 nanoparticles, TiO_2_DL nanoparticles and DL T solution.

TiO_2 crystal phase was not hindered by the addition of lignin during the synthesis. In addition, the average crystallite size of all the nanomaterials, evaluated using the Scherrer equation (eqn (3)), slightly increased from 7 to about 12 nm in the case of the TiO_2_DL200 hybrid due to the greater amount of DL adsorbed onto TiO_2 primary nanoparticles (Table S3†), as previously predicted by N_2 physisorption.

The optical properties of all the nanoparticles were evaluated by means of DRUV analysis (Fig. 3). The spectrum of TiO_2 showed a sigmoidal behaviour and the transmittance increasing from 10% to 100% in the range of 300–400 nm, suggesting a maximum TiO_2 absorption band at around 250 nm, as reported elsewhere.[51] On the other hand, hybrid nanostructures showed transmittance values which decrease by increasing the lignin content within nanoparticles (~50% for TiO_2_DL25, 40% for TiO_2_DL50 and ~20% for TiO_2_DL100 and TiO_2_DL200 nanoparticles in the UV-A region with respect to bare TiO_2 nanostructures). This is a key behaviour related to hybrid nanoparticles, which is not present in the spectra of neat TiO_2 nanoparticles (Fig. 3, blue curve) and of the physical mixture of lignin and TiO_2 (Fig. S8†), thus proving the key role of the molecular combination between lignin and TiO_2 in improving absorption capability, and, therefore, lowering transmission features, in the UV-A/visible region. Therefore, this evidence provides a quantitative result about the possibility for lignin to block UV-A vis light.[57] In addition, an extension of absorption features towards the VIS range is observed as the lignin content grows. This behaviour might be ascribed to lignin absorption features in the visible range. Furthermore, it suggests that DL adsorption on the nanoparticle surface can be due to the complexation of Ti^{4+} ions with lignin phenolic groups, as previously described for other hybrid titania/polyphenol-based nanocomposites.[51,58] As further proof of this, the physical mixing of lignin and TiO_2 nanoparticles only results in a slight visible region absorption increase, which can be attributed exclusively to lignin intrinsic

Table 3 Bandgap values of nanoparticles

Nanoparticles	Bandgap (eV)
TiO_2	≈3.20
TiO_2_DL25	≈3.28
TiO_2_DL50	≈3.32
TiO_2_DL100	≈3.35
TiO_2_DL200	≈3.37

absorption features within that range, as shown in Fig. S8.† Indeed, the transmission profile for bare DL T (Fig. 3, brown curve) exhibited a continuous decrease from visible to UV frequencies, confirming the potential of this phenolic polymer as a strong UV absorbent. This pattern is characteristic of organic fractions such as lignin, which has a brown colour and can absorb in the visible region.

Russo *et al.*[39] demonstrated the presence of a broad visible-range absorbance in the DRS spectra of humic substances/TiO_2 nanostructures which could be ascribable to the co-existence of various electron acceptors and donors within the humic substances. Indeed, this absorbance was probably induced by the near proximity of the electron donors (*i.e.*, polyhydroxylated aromatic and phenol) and the electron acceptors (*i.e.*, quinone) of humic substances within hybrid nanostructures. Therefore, electron donors and acceptors can interact with each other to form a charge-transfer complex. In view of the chemical similarity between humic substances and lignin, these factors can account for the optical properties of TiO_2_DL hybrids.

In addition, the fine conjugation between TiO_2 and DL did not induce a significant change in the energy band gap of semiconductor nanoparticles (Table 3), as shown in previous studies,[39] which could be a direct consequence of the two-fold behavior of lignin acting as both an electron acceptor and donor.

3.2 Functional characterization of hybrid nanoparticles

The quantitative determination of phenolic groups within the nanoparticles and DL T solution was conducted using the Folin–Ciocâlteu assay, following the procedure described in the Experimental section. The results obtained are expressed in terms of mg of gallic acid equivalent, used as a reference standard, per g of sample (Fig. 4 and S9†).

The results revealed a minimal amount of phenolic groups in the TiO_2 sample, which could be attributed to the oxidation phenomenon of the Folin–Ciocâlteu reagent resulting in the formation of a charge transfer complex with TiO_2. It can be observed that the phenolic group content increases by increasing the DL amount during the synthesis, ranging from 10 to about 80 $mg_{GallicAcid}\ g_{sample}^{-1}$ for TiO_2_DL25 and TiO_2_DL200, respectively.

Furthermore, the same test was carried out on bare DL solutions (DL) and on DL solutions in which aqueous lignin solutions were subjected to the same solvothermal treatment carried out in the absence of the inorganic precursor (DL T),
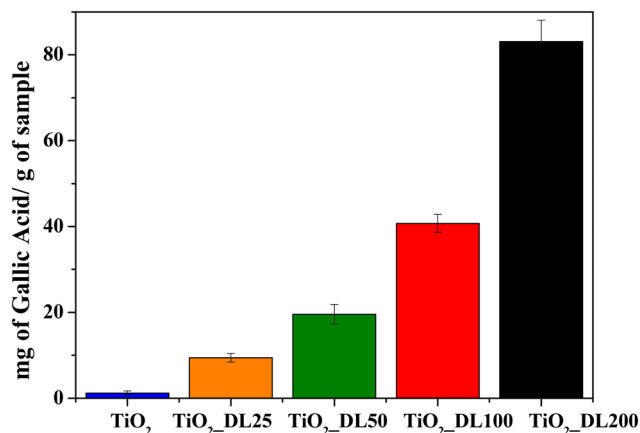
This journal is © The Royal Society of Chemistry 2024

Environ. Sci.: Nano, 2024, **11**, 2127–2144 | **2135**

Fig. 4 Total phenolic content of TiO$_2$ and hybrid TiO$_2$_DL nanoparticles.

Fig. 5 ABTS radical scavenging activity of all synthesized samples.

as described in the Experimental section (Fig. S9†). The results suggest that the quantity of phenolic groups in heat treated samples (DL T100 and DL T200) undergoes a slight increase compared to bare DL solutions (DL 100 and DL 200). Indeed, lignin can undergo slight depolymerization under hydrothermal conditions, leading to the cleavage of ether or ester bonds in its side-chains.[59] Consequently, this fragmentation releases and enhances the accessibility of phenolic groups. This result is in accordance with FTIR and TGA analyses carried out on DL T samples (Fig. S2†), which revealed higher aromatic/polyphenolic groups with respect to DL ones.

Lignin has remarkable antioxidant properties due to its unique chemical structure. Its chemical composition, characterized by a high degree of aromaticity and the presence of various active functional groups such as hydroxyl, carbonyl and methoxyl groups, makes this biopolymer an effective scavenger of free radicals and oxidative species. Indeed, these moieties within lignin biomacromolecules enable them to participate in redox reactions, neutralizing harmful free radicals and preventing oxidative damage. For this reason, lignin is a natural antioxidant that holds great promise for various applications in materials science and bio-sustainable technologies.

The analysis of the antioxidant activity of the samples was conducted using the ABTS assay and the relative results are reported in Fig. 5. The test has been carried out on bare TiO$_2$ and hybrid TiO$_2$ nanoparticles, as well as on DL T solutions to investigate the effective functionality of the hybrid nanostructures.

As expected, neat TiO$_2$ nanoparticles did not show significant antioxidant activity, whereas DL T samples showed good antioxidant activity and the radical scavenging value ranged from 30 to about 65%, by increasing the DL amount within the solutions. However, the best performance is obtained for hybrid nanoparticles, since the radical scavenging values were at least 60% after two minutes, reaching a value of about 90% in the case of the nanoparticles containing the highest amount of DL
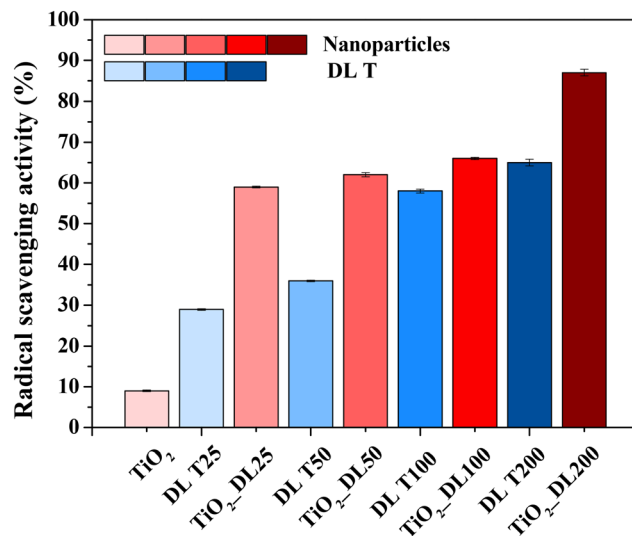
(TiO$_2$_DL200). Therefore, the performance improves with the lignin amount used in the synthesis, suggesting that the degree of antioxidant power related to phenol-based materials depends on the amount of added antioxidant species.[60]

In addition, considering that the test was carried out by using an equal total mass of each sample tested, the antioxidant activity of TiO$_2$_DL nanoparticles appeared to be significantly higher than that of pure DL T solutions, despite containing a much lower DL percentage.

Overall, the combination at the molecular level between lignin and the inorganic precursor during the solvothermal synthesis proved to be a highly effective strategy to improve the intrinsic properties of the organic phase, even if only the hydrothermal treatment led to a slight increase of the phenolic groups in the DL T sample, as suggested by the Folin–Ciocâlteau, FTIR and TGA analyses (Fig. 4 and S2†). As evidence of this, the radical scavenging activity of each hybrid nanostructure is consistently higher than the combined activity of neat TiO$_2$ nanoparticles and the related DL T solutions. To further prove this aspect, the ABTS assay has been carried out on a physical mixture of lignin and titanium dioxide (TiO$_2$ + DL200) (Fig. S10†) in which the amount of organic phase is the same as that contained in the hybrid nanostructures and determined by TGA analysis. For this sample, the radical scavenging activity is approximately 2.3 times lower than that of the hybrid nanoparticles, thus proving the effectiveness of the molecular combination between lignin and TiO$_2$ in improving the antioxidant performance of the organic phase.

Therefore, the possibility for lignin to block UV light and scavenge oxidizing species has been investigated. In addition, to evaluate which of these two phenomena is prevalent, DRUV and ABTS analyses on a physical mixture of lignin and titanium dioxide (TiO$_2$ + DL200) (Fig. S8 and S10†) have been carried out. It is possible to appreciate for the TiO$_2$_DL200

2136 | *Environ. Sci.: Nano*, 2024, **11**, 2127–2144

This journal is © The Royal Society of Chemistry 2024

sample a transmittance value in the UV-A region equal to approximately 20% and in the corresponding physical mixture equal to about 35%. On the other hand, the same sample has an antioxidant activity equal to about 90% (Fig. 5), while the corresponding physical mixture (TiO₂ + DL200) equal to approximately 40%. Therefore, it seems that radical scavenging activity is more prevalent with respect to UV light blocking properties in such a kind of hybrid nanostructure.

The high radical scavenging activity of all the nanoparticles has been confirmed also by means of the DPPH assay as shown in Fig. S11.† Notably, the higher amount of DL incorporation during the synthesis endows TiO₂_DL 100 and TiO₂_DL 200 nanostructures with a relevant antioxidant activity, especially for the TiO₂_DL 200 sample. The antioxidant activity of lignin-based materials is bound to be directly related to the amount of available polyphenols. Even though the latter follows an increasing trend proportional to the growth of lignin content in the samples, as shown by Fig. 4, this is not the case for antioxidant activity, with TiO₂_DL25, TiO₂_DL50 and TiO₂_DL100 exhibiting comparable values, despite the different phenolic contents. This might indicate that some phenol groups are involved in quenching radical species produced by TiO₂ activation under visible light because of the formation of a charge transfer complex with lignin. However, at higher lignin concentrations in the samples, the marked light absorption should shield TiO₂ and limit its photoactivity.

3.3 Antimicrobial and antifungal characterization of hybrid nanoparticles

Evaluating the antimicrobial and antifungal properties of hybrid TiO₂_DL nanoparticles is critical to assess their potential for applications in controlling bacterial and fungal growth, thus addressing public health concerns and advancing environmental remediation solutions. The antimicrobial activity was tested under visible light conditions on both Gram (+) bacteria, including *Staphylococcus aureus (S. aureus)*, *Enterococcus faecalis (E. faecalis)*, *Bacillus cereus (B. cereus)*, and *Listeria monocytogenes (L. monocytogenes)*, and Gram (−) bacteria, including *Salmonella typhi (S. typhi)* and *Escherichia coli (E. coli)*, chosen for their high prevalence and drug resistance. In addition, BSA and AMP + CA have been used as negative and positive controls, respectively (Fig. 6).

All the samples were tested for their antimicrobial activity using the semi-quantitative disk diffusion method (DDK) on the bacterial strains and the results are shown in Fig. 6. The test is characterized by different diffusion of each material in agar in the presence of a specific bacterial strain. When microbial strain is sensitive to the tested samples, the bacterial proliferation is lower, and an inhibition area can be appreciated. As previously stated, the antimicrobial performance of neat TiO₂ nanoparticles under visible irradiation is negligible (Fig. 6). Conversely, the antibacterial
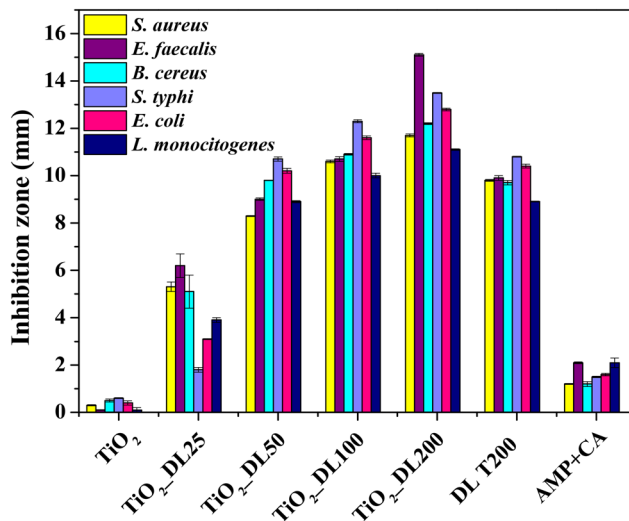

Fig. 6 Inhibition zone (DDK) of all the samples against *S. aureus, E. faecalis, B. cereus, S. typhi, E. coli* and *L. monocytogenes*.

activity of DL T200 and hybrid nanoparticles is much higher than that of AMP + CA, used as a positive control.

In addition, the biocidal efficacy of TiO₂_DL nanohybrids strongly depended on the DL content.[61–63] Also in this case, although the test has been carried out with the same total mass of each sample, the nanostructures that contain a greater amount of lignin, specifically TiO₂_DL100 and TiO₂_DL200 ones, exhibit higher DDK values in comparison to the bare DL T200 solution. Notably, TiO₂_DL200 nanoparticles exhibit DDK values that are approximately 1.5 times higher than the DL T200 sample (Fig. 6), further proving the effectiveness of the fine conjugation between inorganic and organic components in the solvothermal synthesis.

The antimicrobial performance of the nanomaterials has been tested also from a quantitative point of view, by determining the minimum inhibitory concentration (MIC) (Fig. 7). Notably, the MIC value indicates the smallest active concentration of an antibacterial agent that promotes the complete microbial growth inhibition.

The obtained results confirm the negligible antimicrobial performance of neat TiO₂ nanoparticles under visible light irradiation, whose MIC values reached about 6 μg mL⁻¹ (in the case of the *Staphylococcus aureus* bacterial strain). Conversely, the lignin solution after the solvothermal treatment (DL T200) has MIC values almost 4-fold lower than those of the positive control AMP + CA, thus confirming the intrinsic strong antibacterial behavior of neat lignin.

On the other hand, the antimicrobial performance of hybrid nanostructures can be described according to two important features, which totally confirmed DDK results:

I. MIC values of hybrid nanomaterials are lower than those of DL T200 (except in the case of *Enterococcus faecalis*).

II. MIC values of the hybrid nanomaterials decrease as the amount of lignin in the nanomaterial increases (TiO₂_DL200 sample reached an MIC value of about 0.2 μg mL⁻¹ only).

This journal is © The Royal Society of Chemistry 2024

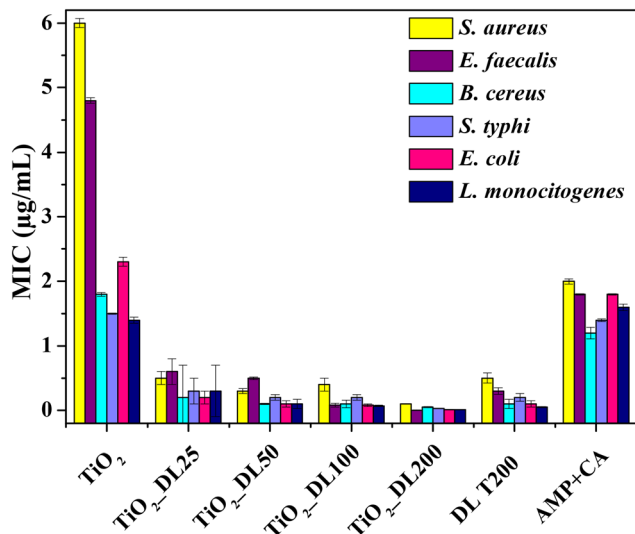*Environ. Sci.: Nano*, 2024, **11**, 2127–2144 | **2137**

Fig. 7 MIC of all the samples against *S. aureus*, *E. faecalis*, *B. cereus*, *S. typhi*, *E. coli* and *L. monocytogenes*.

Several studies have shown that the phenolic groups found in lignin can exert antibacterial action against both Gram (+) and Gram (−) bacteria.[64] However, lignin's antimicrobial activity[65–67] may be mainly related to the extraction method and to the chemical composition of the specific lignin depending on the natural source from which it is obtained.[68]

Although the precise mechanism of action is unknown, it has been proposed that the presence of carboxylic and phenolic groups in the biopolymer leads to an increase in the number of hydrogen bonds with bacterial cell membranes.[56,60,69] This increased affinity is thought to cause irreversible changes in the lipid structure of the membranes,[51] resulting in a decrease in cell wall integrity and increased permeability to reactive oxygen species (ROS), which polyphenol moieties are bound to produce due to their redox active behavior.[51] As a result, not only is pathogenic strain growth slowed, but the activity can also cause bacterial cell death. Moreover, chemical groups in the lignin side chain, such as a double bond between the α and β carbons or a methyl group bound to the γ carbon, could be responsible for the observed noxious effect of lignin against the selected microorganisms.[70] The suppression of the bacterial growth observed here was also related to the inhibition of radical reactions by lignin itself, as suggested by the results of antimicrobial assays and those of antioxidant activity (Fig. 5). Our findings are in line with previous studies reporting the antibacterial efficacy against a variety of pathogenic microorganisms of kraft lignin that possess a high antioxidant capacity.[71,72]

To evaluate any changes in the functionality undergone by neat lignin during the solvothermal process, DDK and MIC tests have been carried out on the solutions before and after the hydrothermal treatment, namely DL200 and DL T200, respectively.

A slight improvement in the functional properties of lignin, possibly due to the increase of aromatic/polyphenolic groups in this sample (Fig. S12, A and B†), can be appreciated, as previously suggested by FTIR and TGA analyses. However, the performance is by far lower than that of comparable amounts of hybrid samples. Overall, the solvothermal process doesn't cause relevant changes in lignin functionalities, even if FTIR and TGA analyses suggested some chemical and thermal differences between DL and DL T samples (Fig. S2†). Indeed, if any compound with smaller molecular weight might be formed during the treatment, it would be washed away during repeated water rinsing and centrifugation of the obtained nanoparticles, thus it should not be responsible for the marked improvement of biocide activity in hybrid samples.

The enhanced antimicrobial activity for hybrid nanoparticles with respect to both lignin solutions (DL 200 and DL T200) could be attributed to several key factors, including nanoparticle specific surface area, size, and morphology, as well as the conformational reorganization of lignin phenolic groups thanks to the fine combination with the inorganic precursor.

Indeed, it could be that DL structural conformation within hybrid nanoparticles, as well as the higher surface area with respect to the bulk lignin, allows for a larger exposure of DL phenolic and hydroxyl groups responsible for better antimicrobial performance.[73]

It has been proposed[13] to develop lignin-based epoxy/TiO_2 hybrid nanoparticles synthesized *via* the liquid deposition method. Their antibacterial performance shows a maximum inhibition zone of 9 mm for the sample containing the same amount of lignin as our TiO_2_DL200 one. In our previous studies,[38,51] we have demonstrated that hybrid humic acid/titanium dioxide nanostructured materials, prepared *via* an *in situ* hydrothermal strategy, display promising antibacterial activity against various pathogens. Indeed, humic acids (HA) can undergo reversible redox reactions; under aerated conditions, semiquinone moieties oxidize, causing electron transfer to O_2 and the generation of OH radicals.[38] Furthermore, catechol moieties in HA could act as ligands for Ti^{4+} ions, forming a ligand-to-metal charge transfer complex (LMCTC) that could cause ROS production by the inorganic phase, even under visible light. In view of the chemical similarity between HA and lignin, these factors can also account for the biocide action of TiO_2_DL hybrids. Therefore, the fine combination of lignin with TiO_2 colloidal suspension during the hydrothermal route is crucial to enhance the intrinsic antimicrobial properties of the organic phase, even under visible light irradiation.

The functionality of the nanomaterials was also evaluated through the assessment of their antifungal activity against two prevalent fungal pathogens, *Candida albicans* (*C. albicans*) and *Aspergillus flavus* (*A. flavus*), by means of MIC analysis. Lignin solution after thermal treatment (DL T200), bare TiO_2 nanoparticles and hybrid nanoparticles were tested, and the results are shown in Fig. 8. In addition, amphotericin B has been used as a positive control.
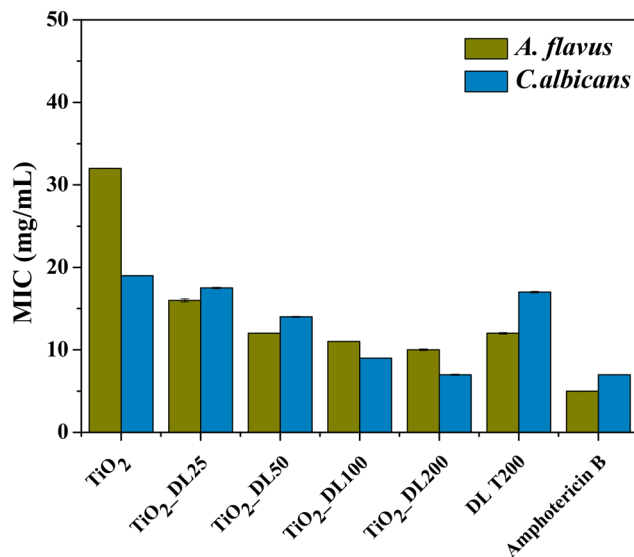
Fig. 8 MIC of all the samples against *Aspergillus flavus* and *Candida albicans*.

The obtained values suggest that neat TiO$_2$ nanoparticles exhibited much lower antifungal performance if compared to the positive control, whereas the DL T200 sample shows higher antifungal performance against *A. flavus*, with respect to the bare TiO$_2$ one, and its activity is comparable to that of bare lignin solution before the hydrothermal treatment, DL 200 (Fig. S12, panel C†). On the other hand, hybrid nanoparticles showed a progressively larger inhibitory effect on fungal proliferation by increasing DL content and this can be explained by different mechanisms[74] related to the release of bioactive compounds responsible for fungal growth inhibition.

Specifically, a more pronounced antifungal effect against *A. flavus* is observed, even at lower organic content, suggesting a varied susceptibility of the tested fungi to the antimicrobial constituents within the samples.

The best antifungal activity has been obtained for the sample with a higher DL amount (TiO$_2$_DL200), whose performance is comparable with that of the positive control. In this case, a very good activity is obtained also against *C. albicans*, for which MIC values decrease about two times with respect to those of neat TiO$_2$ nanoparticles.

Similar to the antimicrobial tests, another important aspect to consider is that antifungal assays were conducted using the same sample concentration in all cases. Therefore, the hybrid nanomaterials achieve once again greater or at least equal antifungal activity compared to that of neat lignin (DL T200) and the positive control, despite containing a much lower DL content (Fig. 8).

The antifungal mechanism of hybrid TiO$_2$_DL nanoparticles could involve the interactions between the phenolic groups and the cell structures of the fungi, leading to deactivation of the cellular enzymes, disruption of fungal cell membranes, inhibition of metabolic processes, or interference with cellular signalling pathways. Thus, the combination of lignin biomacromolecules with an inorganic phase provides a chemical strategy for modulating their chemical functionalities to obtain alternative bioinspired materials with boosted biocide activity thanks to ROS production, which can cause cell dehydration and loss of nutrients.[71,74]

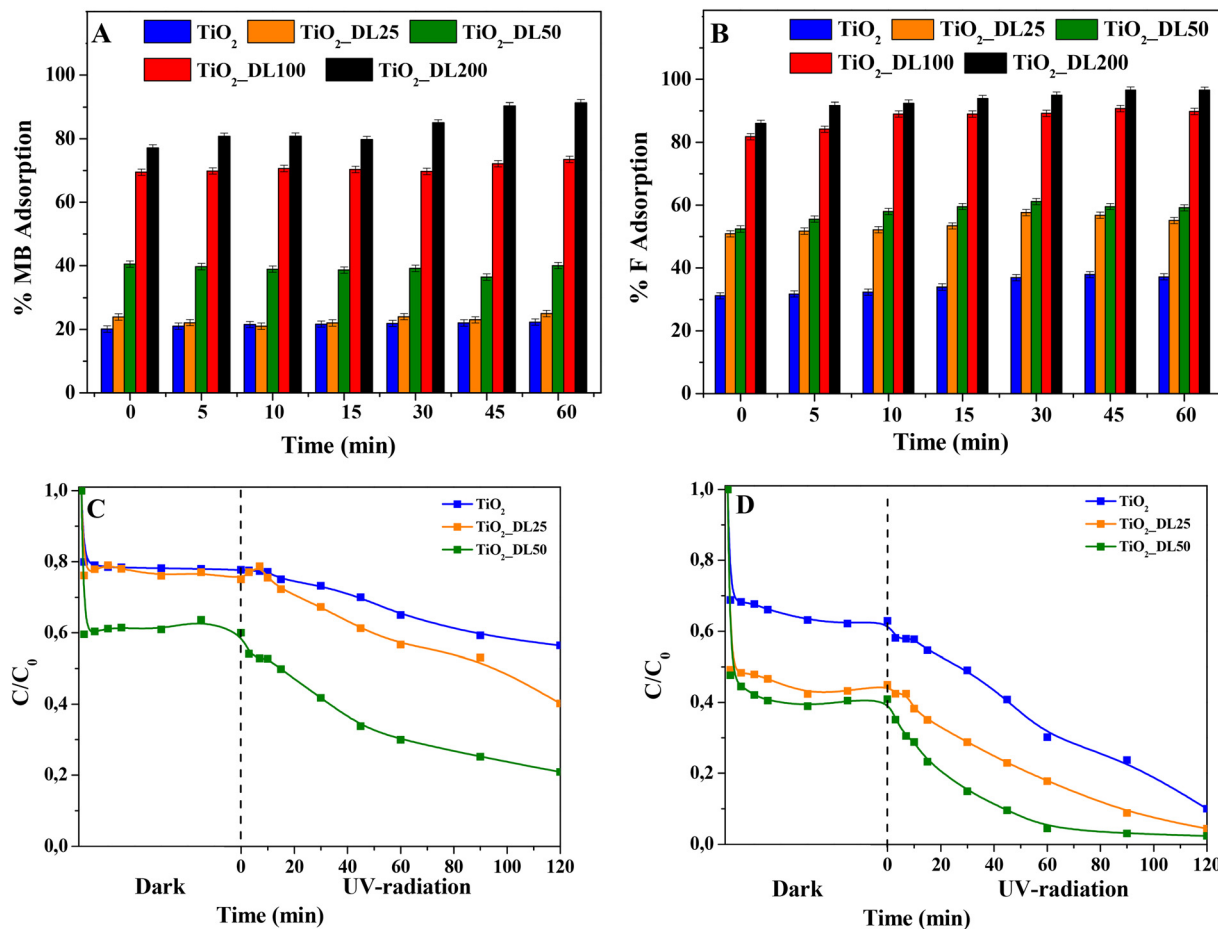## 4. Organic dye removal: adsorption and photocatalytic degradation

To explore the efficacy of TiO$_2$_DL hybrids as active components for water decontamination, the adsorption and photocatalytic activities were tested under UV-A radiation in the presence of MB and F, used as probe dyes. Firstly, the adsorption capacity was assessed in the absence of irradiation. As clearly shown in Fig. 9(A) and (B), among the test samples, TiO$_2$ and TiO$_2$_DL25 presented modest dye adsorption (20–25% and 37–55% for MB and F, respectively), whereas with the increase of DL content within the nanostructures, an increasing marked adsorption was observed, even reaching almost 100% in the case of TiO$_2$_DL200 nanoparticles for both dyes.

A possible explanation of the adsorption can be found in the electrostatic interaction phenomena occurring between the dye molecules and the hybrid nanomaterials. In the case of bare TiO$_2$ nanoparticles, the calculated pH$_{zpc}$ is equal to 7.25, in accordance with previous studies.[75] With the pH of the solution being fixed at 5.0, the material surface is positively charged; furthermore, both MB and F are positively charged;[76] therefore, only a slight interaction between TiO$_2$ nanoparticles and the dye is established, thus resulting in a moderate adsorption. Conversely, in the case of hybrid nanomaterials, the pH$_{zpc}$ of the lignin-based nanomaterials (see Table 4) decreases upon increasing DL content, as determined by the changes in zeta potential values at various pH levels (see Fig. S13†). Indeed, DL is characterized by several functional groups, including carboxyl groups (–COOH), phenol groups (–Ar–OH) and alkoxy phenols (RO–r–OH).[77] At pH 5.0, especially for hybrid nanomaterials with larger DL content, a marked concentration of such functional groups and negative charges on the material surface can be inferred, resulting in a much higher adsorption of the dyes.

Furthermore, to further assess the potential use of the hybrid nanomaterials as adsorbent agents, the adsorption capacity of the TiO$_2$_DL200 sample was compared to that of a material prepared through the physical mixing of lignin and titanium dioxide (TiO$_2$ + DL200). The obtained results (Fig. S14†) indicated a reduced adsorption capacity (80–70% for MB and F, respectively) for the physical mixture nanoparticles (TiO$_2$ + DL200), probably due to the morphological and structural features of the samples, which resulted in less exposure of the active groups.

In addition, the adsorption capacity of TiO$_2$_DL100 and TiO$_2$_DL200 nanoparticles was assessed by varying the initial concentration of both dyes, and the corresponding Langmuir isotherms used to describe the adsorption behavior at a fixed

This journal is © The Royal Society of Chemistry 2024

Environ. Sci.: Nano, 2024, **11**, 2127–2144 | **2139**

Fig. 9 A) % MB and B) % F adsorption (before the irradiation) of the tested nanomaterials. C) MB and D) F adsorption + photocatalytic degradation *vs.* irradiation time under UV + visible light radiation. Experimental conditions: V = 0.05 L; nanocatalyst load = 1000 ppm; [dye] = 6 ppm; UV-A/visible light conditions (where applicable); pH = 5.0; T = 25 °C.

temperature (*i.e.*, 25 °C) are reported in Fig. S15.† The model resulted in good agreement with the experimental data, obtaining an $R^2 > 0.91$ in all cases. The maximum adsorption capacity q_m estimated by the model in the presence of TiO$_2$_DL100 nanoparticles was equal to 1.68 mg g^{-1} and 0.98 mg g^{-1} for MB and F, respectively; in the case of TiO$_2$_DL200, higher values were obtained (14.86 mg g^{-1} and 6.82 mg g^{-1} for MB and F, respectively), due to the higher content of lignin present in the nanomaterials. These values appear lower if compared with those of the usual adsorbents,[78] but they are in accordance with other photocatalytic materials in which the combination of adsorption and photocatalysis was assessed in the removal

of organic dyes.[79] Among the nanomaterials tested, TiO$_2$_DL100 and TiO$_2$_DL200 demonstrated the highest adsorption capacity, obtaining almost 100% dye removal from the solution under dark conditions, thus confirming the enhanced adsorption efficiency reported by others for other lignin-based materials.[80] Conversely, these materials presented poor photocatalytic activity under UV-A radiation (data not shown), probably due to the following reasons:

(i) lignin acts as a natural radical species scavenger, thus reacting with free radicals generated when TiO$_2$ is exposed to UV-A radiation.[81,82] This behaviour is confirmed by the radical scavenging activity determined by ABTS and DPPH assays, which could be responsible for the detrimental impact on the photocatalytic performance of these systems at high amounts of lignin.

(ii) in view of its UV blocking properties, lignin might shield TiO$_2$ from UV-A radiation as driven by optical features of such nanomaterials, investigated by DRUV analysis (Fig. 3).

(iii) the decrease in the specific surface area, pore volume, and average pore diameter observed through BET analysis at surging lignin content (see Table 2).

Table 4 pH$_{zpc}$ of the tested materials

Sample	pH$_{zpc}$
TiO$_2$	7.25
TiO$_2$_DL25	6
TiO$_2$_DL50	5.93
TiO$_2$_DL100	4.87
TiO$_2$_DL200	3.54

(iv) the high amount of adsorbed dye, readily oxidized by the photogenerated radicals, can reduce the impact on the observed dye photodegradation in the solution, monitored during the experiment.

In the case of TiO$_2$, TiO$_2$_DL25 and TiO$_2$_DL50, the lower adsorption ability (and, consequently, lower dye removal efficiency) observed can be possibly overcome by associating adsorption and photocatalysis. For this reason, this possibility was assessed by investigating the photocatalytic behavior of these materials, when irradiated under UV-A radiation. Specifically, % MB and F removal higher than 50% within 120 minutes was observed in the case of the hybrid materials (see Fig. 9(C) and (D)). All the lignin-based nanoparticles demonstrated a higher dye removal efficiency if compared with bare TiO$_2$, with the highest photocatalytic activity recorded in the case of TiO$_2$_DL50. In the case of hybrid nanomaterials, the higher amount of adsorbed dye with respect to bare TiO$_2$ (see the "dark" part in Fig. 9(C) and (D)) can be more readily oxidized by the photogenerated radicals. Yet, at larger lignin amounts (TiO$_2$_DL100 and TiO$_2$_DL_200) UV relevant UV shielding and radical scavenging features decrease the photocatalytic activity. To analyse the photocatalytic degradation data, the pseudo-first order kinetics (Langmuir–Hinshelwood model, see the eqn (7) was applied, obtaining a pseudo-first-order rate constant (k) for all the materials tested (see Fig. 10(A) and (B)). In the case of MB, similar values of the kinetic constants were obtained, ranging between 0.0013 1/min (TiO$_2$) and 0.0038 1/min (TiO$_2$_DL50). Conversely, higher values were obtained in the case of F removal, with the maximum kinetic constant of 0.0132 1/min in the case of TiO$_2$_DL50. The values obtained are in accordance with those reported in the literature for similar systems.[83–85]

Accordingly, these outcomes demonstrate the effectiveness of dye removal in all investigated cases, suggesting the possibility of modulating the adsorption capacity by properly tuning the lignin content within the hybrid nanomaterial.

The reusability of the tested nanomaterials (TiO$_2$_DL100 and TiO$_2$_DL200) as potential adsorbents was assessed in two adsorption cycles (Fig. S16(A) and (B)†), whereas reuse of samples exhibiting significant photocatalytic activity (i.e., TiO$_2$ and TiO$_2$_DL50) was evaluated in three adsorption + photocatalytic cycles (Fig. S17(A) and (B)†). All the tested sorbents showed good stability as sorbents and full reproducibility as photocatalysts towards F removal. On the other hand, a tail off removal efficiency towards MB after each cycle was noticed for the TiO$_2$_DL50 sample. This result could be attributed to the presence of some residues of adsorbed organic byproduct molecules which could not be fully eliminated from the nanomaterial surface during its recovery or to a little DL degradation, as reported by other authors.[86]

Based on our experiments and the information reported in the literature,[87] the overall reaction mechanism for the MB adsorption and photodegradation of the hybrid nanomaterial is proposed in Fig. 11. The synergistic effects of both electrostatic and π–π interactions, as well as the hydrogen bonds between lignin layers and MB dye can explain the adsorption mechanism of this compound on the hybrid nanomaterials, as previously reported.[88] As indicated in the schematic representation (Fig. 11), the organic dye can adsorb on the nanomaterial surface, mainly on the active sites in which lignin is localized. For this reason, a higher lignin content corresponds to a higher adsorption capacity of the hybrid nanomaterial. After the activation of the photocatalytic nanomaterial under UV-A radiation, the electron–hole formation gives rises to different oxidation–reduction reactions, able to form oxidizing species (i.e., O$_2$·$^-$, OH$^-$, OH·), which in turn can oxidize the organic species present in the proximity of the nanomaterial surface.[89] Also in this case, the lignin content plays a key role in the proposed mechanism. Indeed, for a high DL amount within the hybrid nanostructure, the UV-blocking behaviour of the material prevails, thus reducing the concentration of the
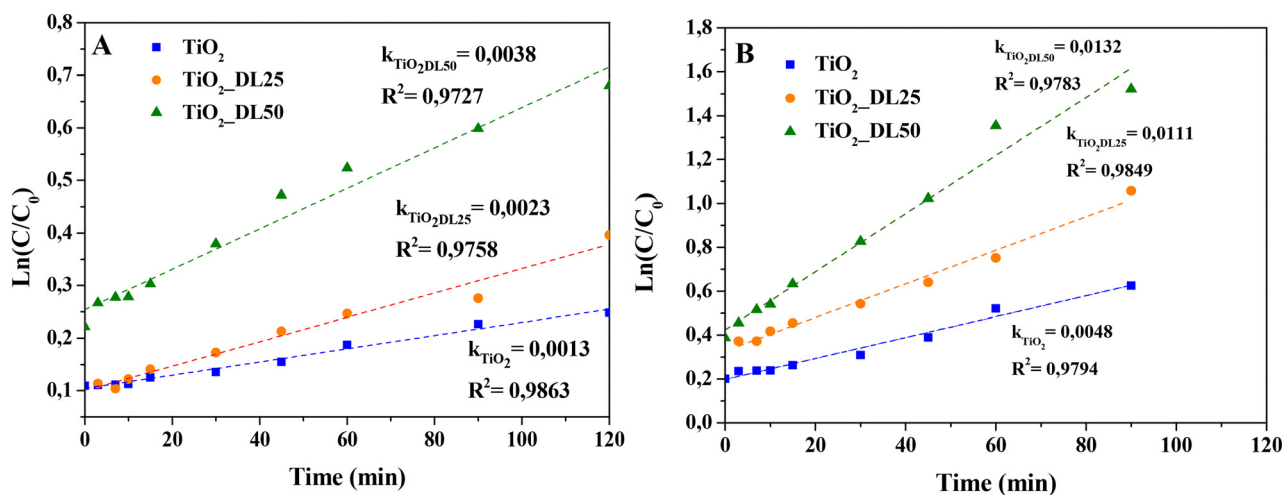

Fig. 10 Pseudo-first-order kinetic modeling of (A) MB and (B) F photodegradation in the presence of different hybrid materials.

This journal is © The Royal Society of Chemistry 2024

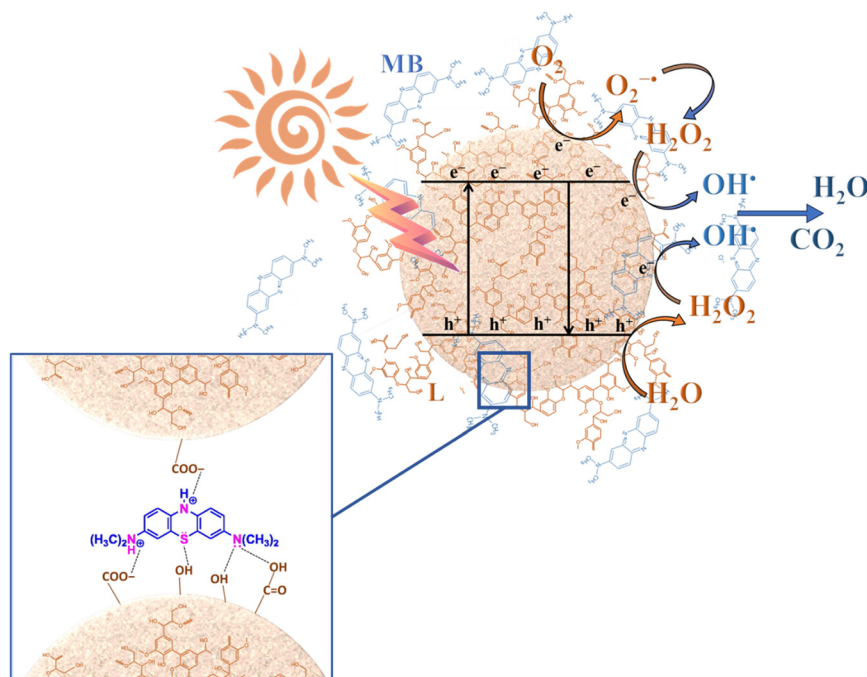*Environ. Sci.: Nano*, 2024, **11**, 2127–2144 | **2141**

Fig. 11 Schematic representation of the adsorption–photodegradation mechanism for MB.

produced photogenerated electrons and holes. Furthermore, the phenolic groups of lignin can scavenge free radicals, thus reducing the oxidation of the organic species (*i.e.*, MB), and, consequently, the photocatalytic efficiency. A similar behaviour can be assumed also for F removal.

Conclusions

In this study, we successfully synthesized hybrid lignin–TiO_2 nanostructured materials using an *in situ* hydrothermal strategy, overcoming key challenges associated with lignin biopolymer exploitation. These materials exhibit a unique molecular-level combination of organic and inorganic components, enhancing and selectively driving the intrinsic properties of the organic phase. The hybrid nanostructures, particularly TiO_2_DL200 nanoparticles with 20% wt of DL, demonstrated a remarkable 90% radical scavenging activity in just 2 minutes and enhanced antibacterial/antimycotic effects. In addition, the obtained nanostructures exhibited high sequestering efficiency and photocatalytic degradation performance towards fuchsin and methylene blue dyes. TiO_2_DL200 nanoparticles showed predominant dye adsorption, reaching almost 100% removal within 5 minutes. Conversely, by reducing the amount of lignin within the nanostructures a trade-off between the adsorption capacity and the photocatalytic activity is achieved, obtaining removal rates higher than 80% in 120 minutes under UV-A conditions in the case of TiO_2_DL50 for both dyes. Moreover, the operational stability of the tested nanomaterials was assessed for different cycles, showcasing the durability and effectiveness of the prepared nanostructures.

Overall, the proposed approach represents a promising eco-sustainable strategy to design multifunctional nanomaterials with simultaneous antioxidant and antimicrobial properties thanks to their ROS scavenging/generating capabilities, as well as promising performance for the adsorption and photodegradation of organic pollutants from wastewater.

The possibility to easily tune the material properties to specific requirements by adjusting the lignin content during the synthesis allows a better exploration of the functionality of synthesised nanostructures. The obtained nanostructures can be effectively used in water decontamination and purification processes, making them an efficient tool for ensuring clean and safe water sources.

Author contributions

Marica Gallo: conceptualization, methodology, investigation, data curation. Virginia Venezia, Marica Muscetta: conceptualization, methodology, data curation, writing – original draft, supervision. Rossella Grappa, Mariavittoria Verrillo: methodology, data curation. Gianluca Landi: investigation, writing – review & editing. Raffaele Marotta: conceptualization, writing – review & editing. Giuseppina Luciani: writing – review & editing, supervision, project administration. All authors have read and agreed to the published version of the manuscript.

Conflicts of interest

The authors declare that they have no known competing financial interests or personal relationships that could have appeared to influence the work reported in this paper.

Acknowledgements

References

1 A. Ncube, S. Mtetwa, M. Bukhari, G. Fiorentino and R. Passaro, *Energies*, 2023, **16**(4), 1752.

2 A. Saravanan, S. Karishma, P. Senthil Kumar and G. Rangasamy, *Fuel*, 2023, **338**, 127221.

3 A. Jain, S. Sarsaiya, M. Kumar Awasthi, R. Singh, R. Rajput, U. C. Mishra, J. Chen and J. Shi, *Fuel*, 2022, **307**, 121859.

4 V. Ashokkumar, G. Flora, R. Venkatkarthick, K. SenthilKannan, C. Kuppam, G. Mary Stephy, H. Kamyab, W. H. Chen, J. Thomas and C. Ngamcharussrivichai, *Fuel*, 2022, **324**, 124313.

5 M. K. Awasthi, T. Sar, S. C. Gowd, K. Rajendran, V. Kumar, S. Sarsaiya, Y. Li, R. Sindhu, P. Binod, Z. Zhang, A. Pandey and M. J. Taherzadeh, *Fuel*, 2023, **342**, 127790.

6 M. Erfani Jazi, G. Narayanan, F. Aghabozorgi, B. Farajidizaji, A. Aghaei, M. A. Kamyabi, C. M. Navarathna and T. E. Mlsna, *SN Appl. Sci.*, 2019, **1**, 1–19.

7 W. Yang, Y. Qu, B. Zhou, C. Li, L. Jiao and H. Dai, *Ind. Crops Prod.*, 2021, **171**, 113848.

8 V. Venezia, M. Verrillo, N. Gallucci, R. Di Girolamo, G. Luciani, G. D'errico, L. Paduano, A. Piccolo and G. Vitiello, *J. Environ. Chem. Eng.*, 2023, **11**, 108973.

9 A. Kylili, M. Koutinas, P. Z. Georgali and P. A. Fokaides, *International Journal of Sustainable Energy*, 2023, **42**(1), 1008–1027.

10 E. Lichtfouse, J. Schwarzbauer and D. Robert, *Environmental chemistry : green chemistry and pollutants in ecosystems*, Springer, 2005.

11 M. J. John, M. C. Lefatle and B. Sithole, *Sustainable Chem. Pharm.*, 2022, **25**, 100594.

12 Y. Sun, T. Wang, X. Sun, L. Bai, C. Han and P. Zhang, *Ind. Crops Prod.*, 2021, **166**, 113473.

13 J. Yang, J. Dai, X. Liu, S. Fu, E. Zong and P. Song, *Int. J. Biol. Macromol.*, 2022, **210**, 85–93.

14 V. B. Ruthran, P. Barman, R. Kadam and A. Kumar, *Emergent Mater.*, 2021, **5**, 923–943.

15 M. Sajjadi, F. Ahmadpoor, M. Nasrollahzadeh and H. Ghafuri, *Int. J. Biol. Macromol.*, 2021, **178**, 394–423.

16 G. Parvathy, A. S. Sethulekshmi, J. S. Jayan, A. Raman and A. Saritha, *Process Saf. Environ. Prot.*, 2021, **145**, 395–410.

17 H. Wang, H. Cao, H. Wu, Q. Zhang, X. Mao, L. Wei, F. Zhou, R. Sun and C. Liu, *ACS Appl. Nano Mater.*, 2023, **6**, 14165–14176.

18 L. K. De Oliveira, E. F. Molina, A. L. A. Moura, E. H. De Faria and K. J. Ciuffi, *ACS Appl. Mater. Interfaces*, 2016, **8**, 1478–1485.

19 P. Amato, M. Muscetta, V. Venezia, M. Cocca, G. Gentile, R. Castaldo, R. Marotta and G. Vitiello, *J. Environ. Chem. Eng.*, 2023, **11**(1), 109003.

20 X. Zhou, E. Liu, J. Li, F. Chen, Y. Zhang, K. Chen and D. Qi, *ACS Appl. Nano Mater.*, 2023, **6**(16), 14820–14830.

21 D. Yang, S. Wang, R. Zhong, W. Liu and X. Qiu, *Front. Chem. Sci. Eng.*, 2019, **13**, 59–69.

22 M. Andrade-Guel, C. Cabello-Alvarado, C. A. Avila-Orta, M. Pérez-Alvarez, G. Cadenas-Pliego, P. Y. Reyes-Rodríguez and L. Rios-González, *Polymers*, 2022, **14**(7), 1300.

23 K. Bula, P. Jędrzejczak, D. Ajnbacher, M. N. Collins and Ł. Klapiszewski, *Int. J. Biol. Macromol.*, 2023, **246**, 125626.

24 R. Kaur, N. S. Thakur, S. Chandna and J. Bhaumik, *ACS Sustainable Chem. Eng.*, 2021, **9**, 11223–11237.

25 K. Chen, X. Zhou, D. Wang, J. Li and D. Qi, *Int. J. Biol. Macromol.*, 2022, **218**, 33–43.

26 K. M. Samb-Joshi, Y. A. Sethi, A. A. Ambalkar, H. B. Sonawane, S. P. Rasale, R. P. Panmand, R. Patil, B. B. Kale and M. G. Chaskar, *J. Compos. Sci.*, 2019, **3**(3), 90.

27 D. Piccinino, E. Capecchi, E. Tomaino, S. Gabellone, V. Gigli, D. Avitabile and R. Saladino, *Antioxidants*, 2021, **10**, 1–19.

28 J. C. Colmenares, R. S. Varma and P. Lisowski, *Green Chem.*, 2016, **18**, 5736–5750.

29 A. Khan, M. Goepel, W. Lisowski, D. Łomot, D. Lisovytskiy, M. Mazurkiewicz-Pawlicka, R. Gläser and J. C. Colmenares, *RSC Adv.*, 2021, **11**, 34996–35010.

30 G. Zhai, J. Zhou, M. Xie, C. Jia, Z. Hu, H. Xiang and M. Zhu, *Adv. Sustainable Syst.*, 2023, **7**(4), 2200459.

31 R. Kaur, S. K. Bhardwaj, S. Chandna, K. H. Kim and J. Bhaumik, *J. Cleaner Prod.*, 2021, **317**, 128300.

32 J. Yu, L. Li, Y. Qian, H. Lou, D. Yang and X. Qiu, *Ind. Eng. Chem. Res.*, 2018, **57**, 15740–15748.

33 Ł. Klapiszewski, K. Siwińska-Stefańska and D. Kołodyńska, *Chem. Eng. J.*, 2017, **314**, 169–181.

34 N. Srisasiwimon, S. Chuangchote, N. Laosiripojana and T. Sagawa, *ACS Sustainable Chem. Eng.*, 2018, **6**, 13968–13976.

35 Y. Fu, X. Liu and G. Chen, *Results Phys.*, 2019, **12**, 405–411.

36 R. Al-Tohamy, S. S. Ali, F. Li, K. M. Okasha, Y. A. G. Mahmoud, T. Elsamahy, H. Jiao, Y. Fu and J. Sun, *Ecotoxicol. Environ. Saf.*, 2022, **231**, 113160.

37 M. Hassanpour, H. Safardoust-Hojaghan and M. Salavati-Niasari, *J. Mol. Liq.*, 2017, **229**, 293–299.

38 G. Vitiello, V. Venezia, M. Verrillo, A. Nuzzo, J. Houston, S. Cimino, G. D'Errico, A. Aronne, L. Paduano, A. Piccolo and G. Luciani, *Environ. Res.*, 2021, **193**, 110562.

39 S. Russo, M. Muscetta, P. Amato, V. Venezia, M. Verrillo, R. Rega, S. Lettieri, M. Cocca, R. Marotta and G. Vitiello, *Chemosphere*, 2024, **346**, 140605.

40 F. Moccia, S. Agustin-Salazar, L. Verotta, E. Caneva, S. Giovando, G. D'Errico, L. Panzella, M. D'Ischia and A. Napolitano, *Antioxidants*, 2020, **9**(5), 438.

41 V. Venezia, G. Pota, B. Silvestri, G. Vitiello, P. Di Donato, G. Landi, V. Mollo, M. Verrillo, S. Cangemi, A. Piccolo and G. Luciani, *Chemosphere*, 2022, **287**, 131985.

42 M. Verrillo, M. Salzano, V. Cozzolino, R. Spaccini and A. Piccolo, *Waste Manage.*, 2021, **120**, 98–107.

This journal is © The Royal Society of Chemistry 2024

Environ. Sci.: Nano, 2024, **11**, 2127–2144 | **2143**

43 A. Panáček, M. Kolář, R. Večeřová, R. Prucek, J. Soukupová, V. Kryštof, P. Hamal, R. Zbořil and L. Kvítek, *Biomaterials*, 2009, **30**, 6333–6340.

44 E. Pinto, M. Lago, L. Branco, L. A. Vale-Silva and M. D. Pinheiro, *Mycopathologia*, 2014, **177**, 157–166.

45 E. S. Gorman and M. R. Shnider, *Effect of methylene blue on the absorbance of solutions of haemoglobin*, 1988, vol. 60.

46 Z. Durmus, B. Z. Kurt and A. Durmus, *ChemistrySelect*, 2019, **4**, 271–278.

47 J. Avossa, G. Pota, G. Vitiello, A. Macagnano, A. Zanfardino, M. Di Napoli, A. Pezzella, G. D'Errico, M. Varcamonti and G. Luciani, *Mater. Sci. Eng., C*, 2021, **123**, 111954.

48 L. El Fels, M. Zamama and M. Hafidi, in *Biodegradation and Bioremediation of Polluted Systems - New Advances and Technologies*, InTech, 2015.

49 S. Yu, M. Xie, Q. Li, Y. Zhang and H. Zhou, *J. Energy Inst.*, 2022, **103**, 147–153.

50 X. Chen, H. Li, S. Sun, X. Cao and R. Sun, *Sci. Rep.*, 2016, **6**(1), 39354.

51 V. Venezia, C. Prieto, Z. Evtoski, C. Marcoaldi, B. Silvestri, G. Vitiello, G. Luciani and J. M. Lagaron, *J. Ind. Eng. Chem.*, 2023, **124**, 510–522.

52 L.-M. Liu, S.-C. Li, H. Cheng, U. Diebold and A. Selloni, *J. Am. Chem. Soc.*, 2011, **133**, 7816–7823.

53 Z. Xiao, P. Guo and N. Sun, *J. Appl. Polym. Sci.*, 2017, **134**(2), DOI: 10.1002/app.44377.

54 M. H. Sipponen, H. Lange, M. Ago and C. Crestini, *ACS Sustainable Chem. Eng.*, 2018, **6**, 9342–9351.

55 L. Chen, S.-M. Luo, C.-M. Huo, Y.-F. Shi, J. Feng, J.-Y. Zhu, W. Xue and X. Qiu, *Green Chem.*, 2022, **24**, 285–294.

56 Z. Zhang, M. Chen, Y. Yu, S. Pan and Y. Liu, *Antimicrob. Resist. Infect. Control*, 2018, **7**, 1–13.

57 K. M. Reddy, S. V. Manorama and A. R. Reddy, *Bandgap studies on anatase titanium dioxide nanoparticles*, 2002, vol. 78.

58 H. Ou-Yang, G. Stamatas and N. Kollias, *J. Invest. Dermatol.*, 2004, **122**, 492–496.

59 H. Y. Li, B. Wang, J. L. Wen, X. F. Cao, S. N. Sun and R. C. Sun, *Energy Convers. Manage.*, 2018, **155**, 58–67.

60 K. J. Figueroa-Lopez, A. A. Vicente, M. A. M. Reis, S. Torres-Giner and J. M. Lagaron, *Nanomaterials*, 2019, **9**(2), 144.

61 Z. Huang, Z. Zeng, Z. Song, A. Chen, G. Zeng, R. Xiao, K. He, L. Yuan, H. Li and G. Chen, *J. Hazard. Mater.*, 2020, **383**, 121153.

62 E. Beetge, J. Du Plessis, D. Gerbrandt, M. Ller, C. Goosen and F. Janse Van Rensburg, *The influence of the physicochemical characteristics and pharmacokinetic properties of selected NSAID's on their transdermal absorption*, 2000, vol. 193.

63 R. Ansorg and W. Rochus, *Arzneimittelforschung*, 1978, **28**, 2195–2198.

64 F. C. Lobo, E. M. Franco, E. M. Fernandes and R. L. Reis, *Molecules*, 2021, **26**(6), 1749.

65 A. Alzagameem, S. E. Klein, M. Bergs, X. T. Do, I. Korte, S. Dohlen, C. Hüwe, J. Kreyenschmidt, B. Kamm, M. Larkins and M. Schulze, *Polymers*, 2019, **11**(4), 670.

66 S. E. Klein, A. Alzagameem, J. Rumpf and I. Korte, J. Kreyenschmidt and M. Schulze, *Coatings*, 2019, **9**(8), 494.

67 S. Mearaj, A. M. Ajaz, T. M. Kim and J. W. Choi, *ACS Appl. Bio Mater.*, 2023, **6**, 3648–3660.

68 P. Figueiredo, K. Lintinen, J. T. Hirvonen, M. A. Kostiainen and H. A. Santos, *Prog. Mater. Sci.*, 2018, **93**, 233–269.

69 N. P. Gamedze, M. N. Mthiyane, S. Mavengahama, M. Singh and D. C. Onwudiwe, *Chem. Afr.*, 2023, 1–10.

70 J. L. Espinoza-Acosta, P. I. Torres-Chávez, B. Ramírez-Wong, C. M. López-Saiz and B. Montaño-Leyva, *BioResources*, 2016, **11**(2), 5452–5481.

71 M. Verrillo, D. Savy, S. Cangemi, C. Savarese, V. Cozzolino and A. Piccolo, *J. Sci. Food Agric.*, 2022, **102**, 2885–2892.

72 X. Dong, M. Dong, Y. Lu, A. Turley, T. Jin and C. Wu, *Ind. Crops Prod.*, 2011, **34**, 1629–1634.

73 M. Morsali, A. Moreno, A. Loukovitou, I. Pylypchuk and M. H. Sipponen, *Biomacromolecules*, 2022, **23**, 4597–4606.

74 N. Miura and Y. Shinohara, *Biochem. Biophys. Res. Commun.*, 2009, **390**, 733–737.

75 H. Trabelsi, G. P. Atheba, O. Hentati, Y. Dezirée Mariette, D. Robert, P. Drogui and M. Ksibi, *J. Adv. Oxid. Technol*, 2016, **19**, 79.

76 National Center for Biotechnology Information, *PubChem Compound Summary for CID 6099, Methylene Blue*, Retrieved November 29, 2023.

77 A. P. Richter, B. Bharti, H. B. Armstrong, J. S. Brown, D. Plemmons, V. N. Paunov, S. D. Stoyanov and O. D. Velev, *Langmuir*, 2016, **32**, 6468–6477.

78 X. J. Liu, M. F. Li, J. F. Ma, J. Bian and F. Peng, *Colloids Surf., A*, 2022, **642**, 128621.

79 A. Kumar, S. Kumar, A. Bahuguna, A. Kumar, V. Sharma and V. Krishnan, *Mater. Chem. Front.*, 2017, **1**, 2391–2404.

80 T. Masilompane, N. Chaukura, A. K. Mishra, S. B. Mishra and B. B. Mamba, *Bio-and Nanosorbents from Natural Resources*, 2018, pp. 55–73.

81 M. H. Tran, D. P. Phan and E. Y. Lee, *Green Chem.*, 2021, **23**, 4633–4646.

82 Y. Li, D. Yang, S. Lu, X. Qiu, Y. Qian and P. Li, *ACS Sustainable Chem. Eng.*, 2019, **7**, 6234–6242.

83 L. Barrientos, P. Allende, M. Á. Laguna-Bercero, J. Pastrián, J. Rodriguez-Becerra and L. Cáceres-Jensen, *J. Phys. Chem. Solids*, 2018, **119**, 147–156.

84 A. Singh Vig, A. Gupta and O. P. Pandey, *Adv. Powder Technol.*, 2018, **29**, 2231–2242.

85 L. Saikia, D. Bhuyan, M. Saikia, B. Malakar, D. K. Dutta and P. Sengupta, *Appl. Catal., A*, 2015, **490**, 42–49.

86 X. Chen, H. Sun, J. Zhang, O. Ahmed Zelekew, D. Lu, D. H. Kuo and J. Lin, *Appl. Catal., B*, 2019, **252**, 152–163.

87 O. Blank, E. Davioud-Charvet and M. Elhabiri, *Antioxid. Redox Signaling*, 2012, **17**, 544–554.

88 Y. Xie, B. Yan, H. Xu, J. Chen, Q. Liu, Y. Deng and H. Zeng, *ACS Appl. Mater. Interfaces*, 2014, **6**, 8845–8852.

89 P. O. Oladoye, T. O. Ajiboye, E. O. Omotola and O. J. Oyewola, *Results Eng.*, 2022, **16**, 100678.

2144 | *Environ. Sci.: Nano*, 2024, **11**, 2127–2144

This journal is © The Royal Society of Chemistry 2024